Electronic Supplementary Material (ESI) for Energy & Environmental Science.
This journal is © The Royal Society of Chemistry 2024

Supplementary Information

Restructuring of aqueous electrolytes using soft-acidic/hard-basic zwitterion for low-temperature anode-free Zn batteries

Hong-I Kim,[a,‡] Kyung Min Lee,[b,‡] Won-Yeong Kim,[a] Seong Hyeon Kweon,[b] Xiao Wang,[c] Shuanghao Zheng,[c] Seung-Hyeok Kim,[a] Jee Ho Ha,[b] Seok Ju Kang,[b] Zhong-Shuai Wu,[c,*] Sang Kyu Kwak,[e,**] and Sang-Young Lee[a,***]

[a]Department of Chemical and Biomolecular Engineering, Yonsei University, 50 Yonsei-ro, Seodaemun-gu, Seoul, 03722, Republic of Korea

[b]Department of Energy Engineering, School of Energy and Chemical Engineering, Ulsan National Institute of Science and Technology (UNIST), Ulsan 44919, Republic of Korea

[c]State Key Laboratory of Catalysis, Dalian National Laboratory for Clean Energy, Dalian Institute of Chemical Physics Chinese Academy of Sciences, 457 Zhongshan Road, Dalian 116023, China

[d]Department of Chemical and Biological Engineering, Korea University, 145 Anam-ro, Seongbuk-gu, Seoul 02841, Republic of Korea

‡These authors contributed equally.

*Correspondence: wuzs@dicp.ac.cn

**Correspondence: skkwak@korea.ac.kr

***Correspondence: syleek@yonsei.ac.kr

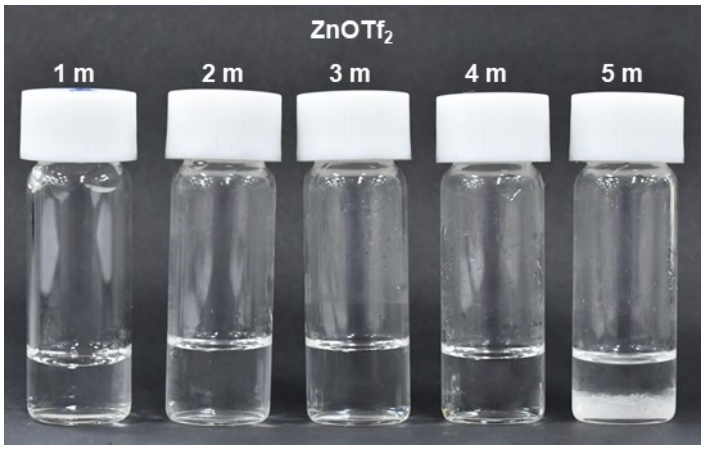

Fig. S1. Photographs of the various aqueous electrolytes at room temperature: $Zn(OTf)_2$ in water.

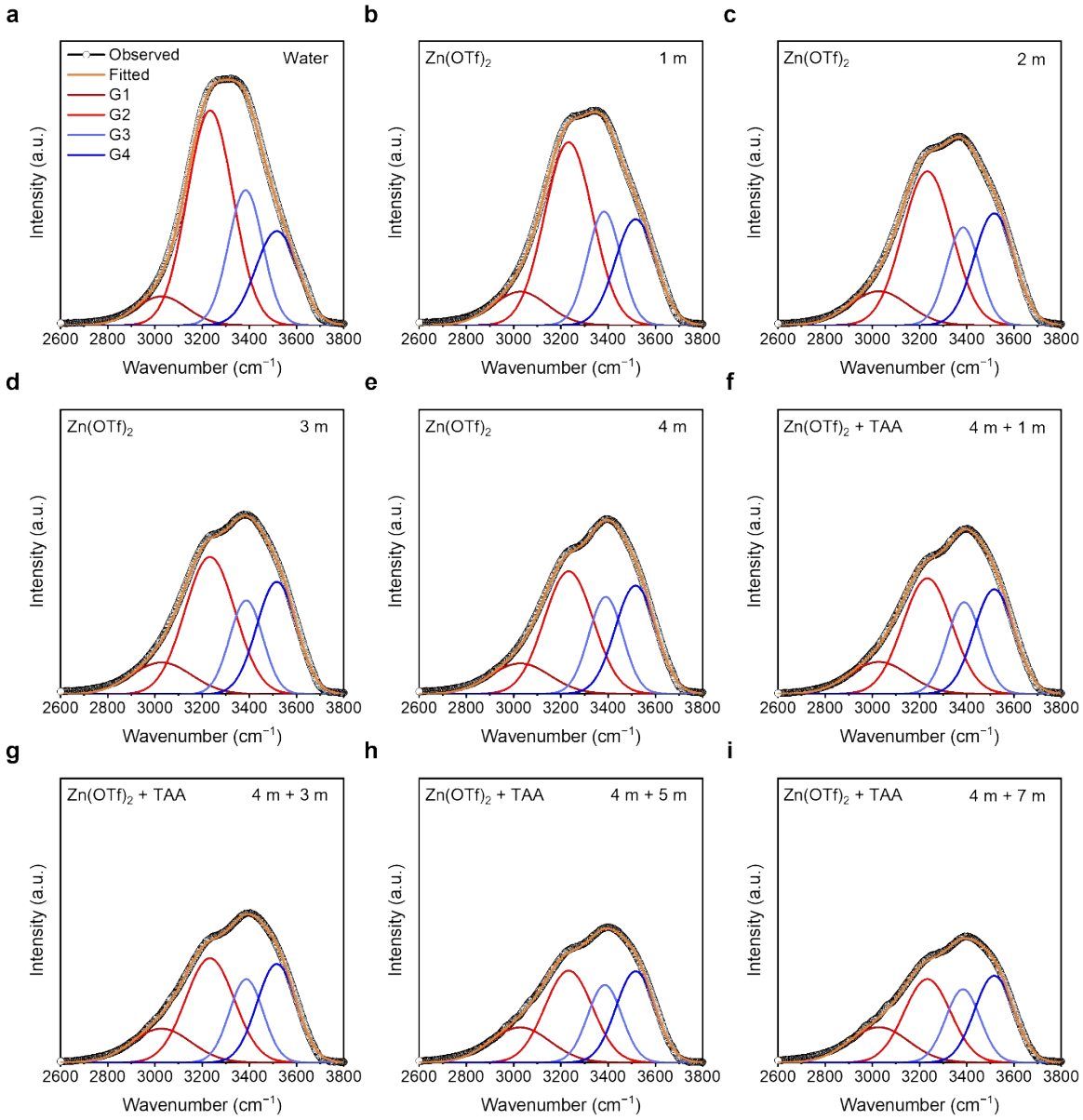

* Concentrations are denoted as *x* m + *y* m, where *x* is concentration of $Zn(OTf)_2$ and *y* as that of TAA

Fig. S2. Peak-fitting of the FT-IR spectra for the O−H stretching vibration in the various aqueous electrolytes: water (**a**), 1 m $Zn(OTf)_2$ (**b**), 2 m $Zn(OTf)_2$ (**c**), 3 m $Zn(OTf)_2$ (**d**), 4 m $Zn(OTf)_2$ (**e**), 4 m $Zn(OTf)_2$ + 1 m TAA (**f**), 4 m $Zn(OTf)_2$ + 3 m TAA (**g**), 4 m $Zn(OTf)_2$ + 5 m TAA (**h**) and 4 m $Zn(OTf)_2$ + 7 m TAA (**i**). The concentrations of the aqueous electrolytes are denoted as *x* m + *y* m, where *x* and *y* are the concentrations of $Zn(OTf)_2$ and TAA, respectively.

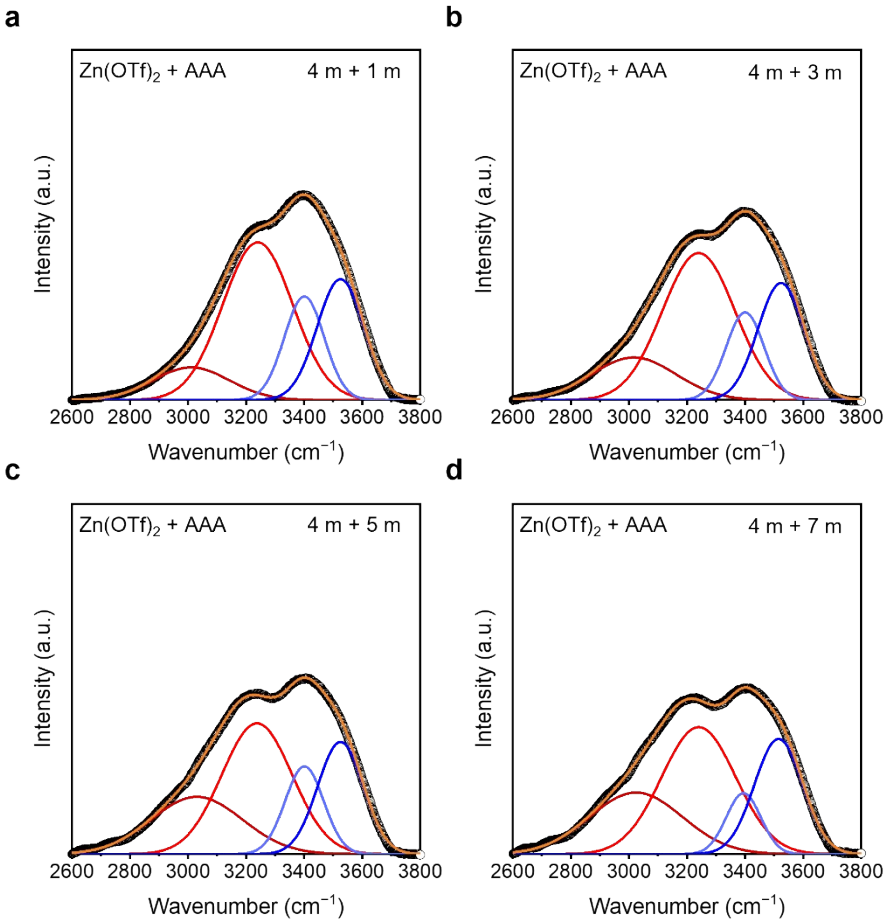

* Concentrations are denoted as *x* m + *y* m, where *x* is concentration of $Zn(OTf)_2$ and *y* as that of AAA

Fig. S3. Peak-fitting of the FT-IR spectra for the O−H stretching vibration in the various aqueous electrolytes: 4 m $Zn(OTf)_2$ + 1 m AAA (**a**), 4 m $Zn(OTf)_2$ + 3 m AAA (**b**), 4 m $Zn(OTf)_2$ + 5 m AAA (**c**) and 4 m $Zn(OTf)_2$ + 7 m AAA (**d**). The concentrations of the aqueous electrolytes are denoted as *x* m + *y* m, where *x* and *y* are the concentrations of $Zn(OTf)_2$ and AAA, respectively.

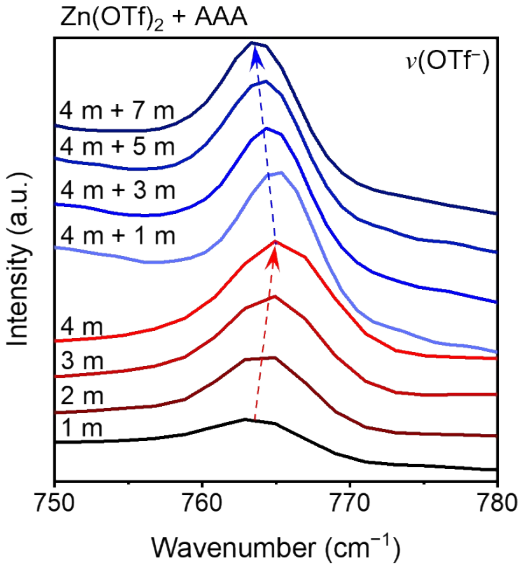

Fig. S4. FT-IR spectra for the OTf^- stretching vibration of anions in the various aqueous electrolytes as a function of $ZnOTf_2$ and AAA concentration.

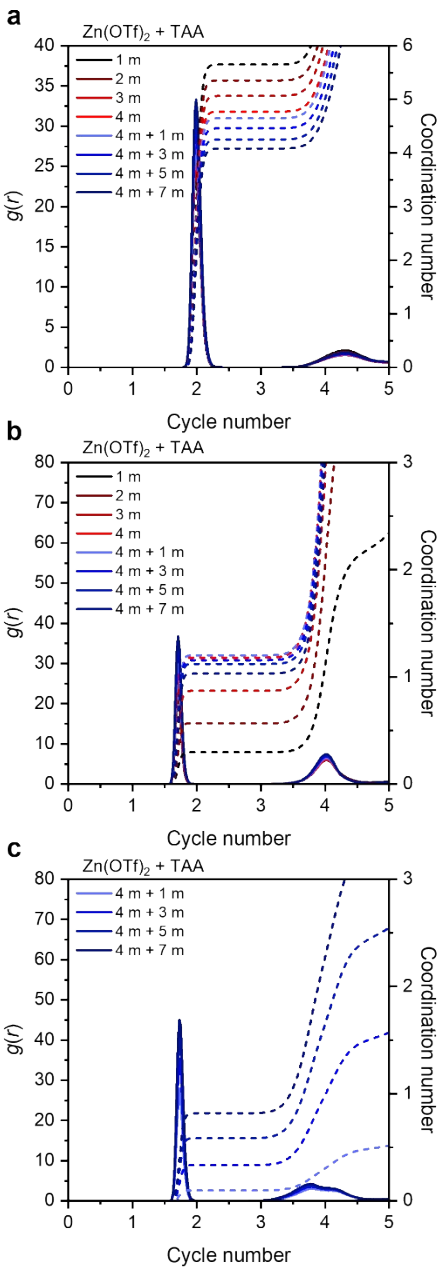

Fig. S5. RDF profiles of the water molecules **(a)**, OTf^- **(b)**, and TAA molecules **(c)** in the Zn^{2+} solvation sheath as a function of $ZnOTf_2$ and TAA concentration. The average values of the RDF and CN are obtained from the three independent MD trajectories. The concentrations of the aqueous electrolytes are denoted as *x* m + *y* m, where *x* and *y* are the concentrations of $Zn(OTf)_2$ and TAA, respectively.

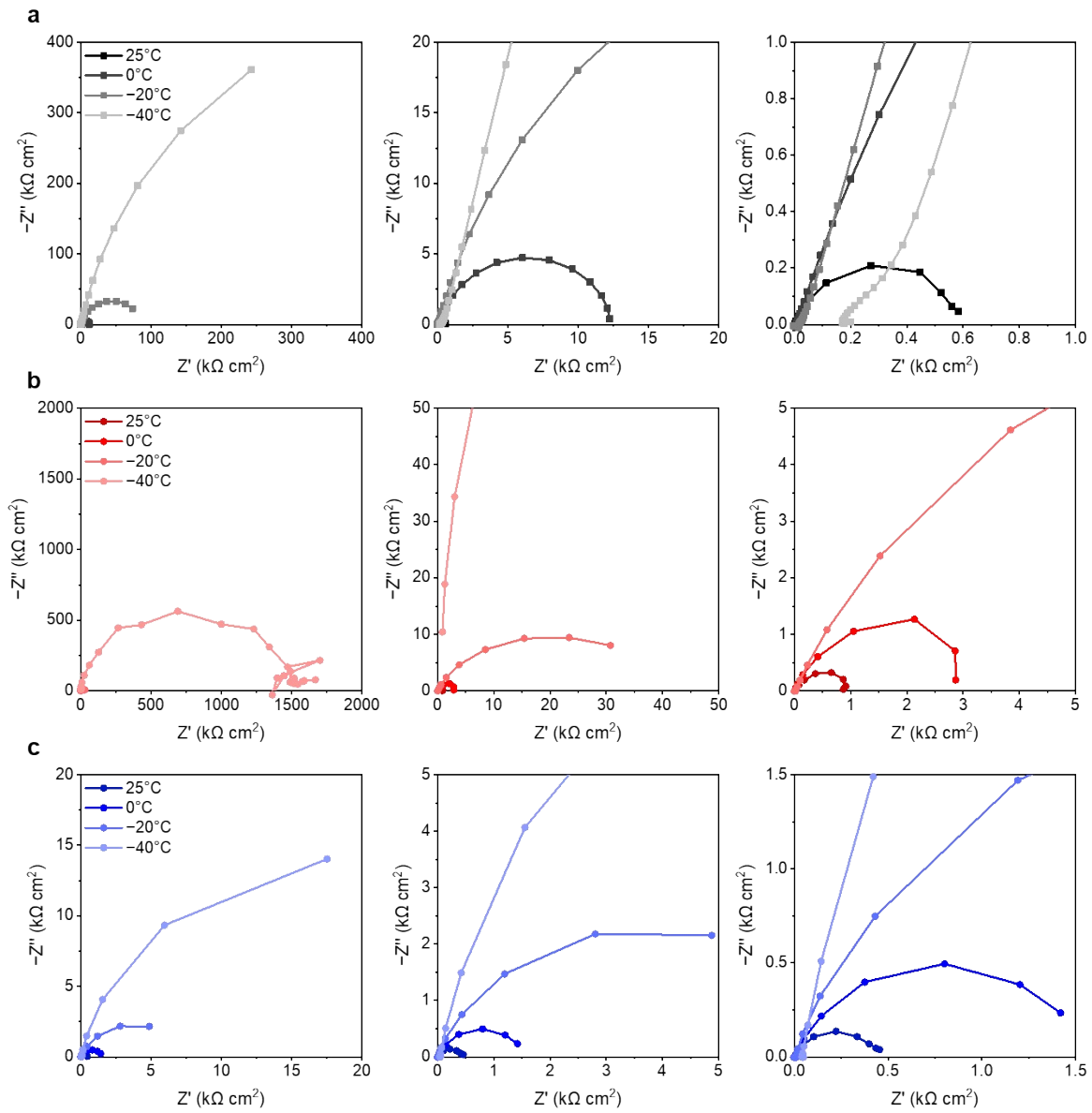

Fig. S6. EIS profiles of the Zn||Zn symmetric cells as a function of temperature in 1 m $Zn(OTf)_2$ electrolyte (**a**), 4 m $Zn(OTf)_2$ electrolyte (**b**), and ZT-electrolyte (**c**).

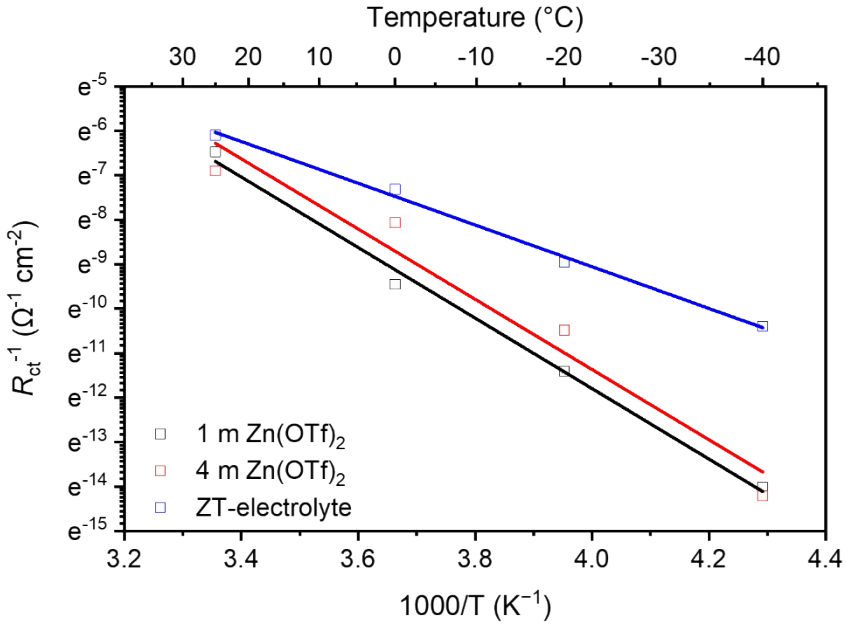

Fig. S7. Arrhenius plot of the R_{ct} for the Zn||Zn symmetric cells in the different aqueous electrolytes.

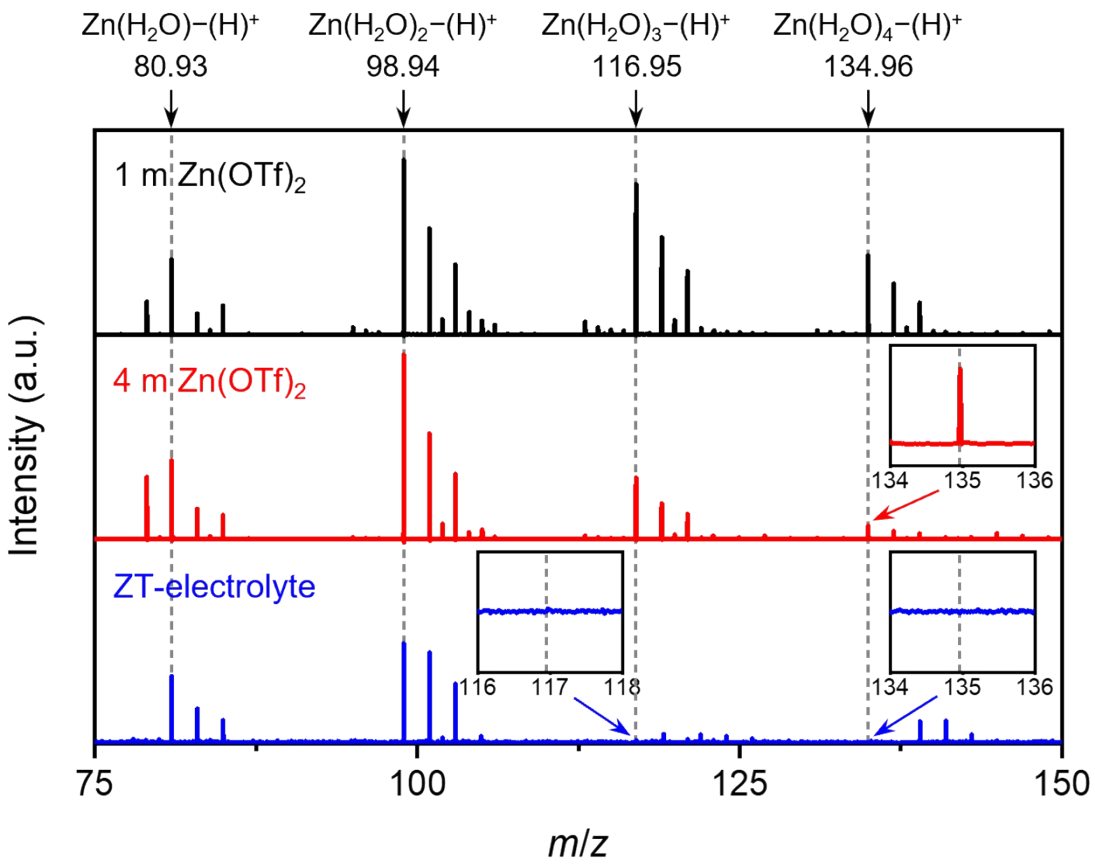

Fig. S8. Electrospray ionization mass (ESI-MS) spectra of the different aqueous electrolytes used to identify the coordination complexes of the Zn^{2+} solvation sheath.

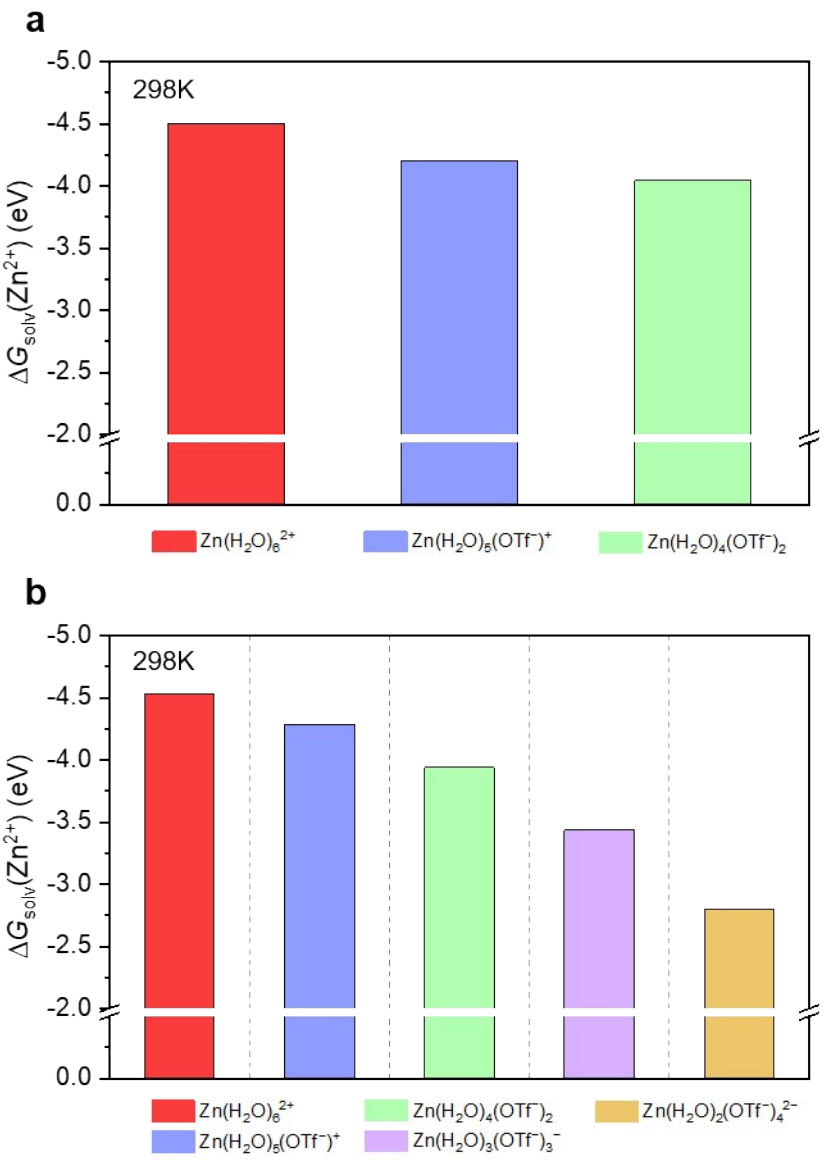

Fig. S9. Solvation free energy (ΔG_{solv}) of the Zn^{2+} in the solvation sheath as a function of coordination complex: 1 m $Zn(OTf)_2$ electrolyte (**a**) and 4 m $Zn(OTf)_2$ electrolyte (**b**) at 298K.

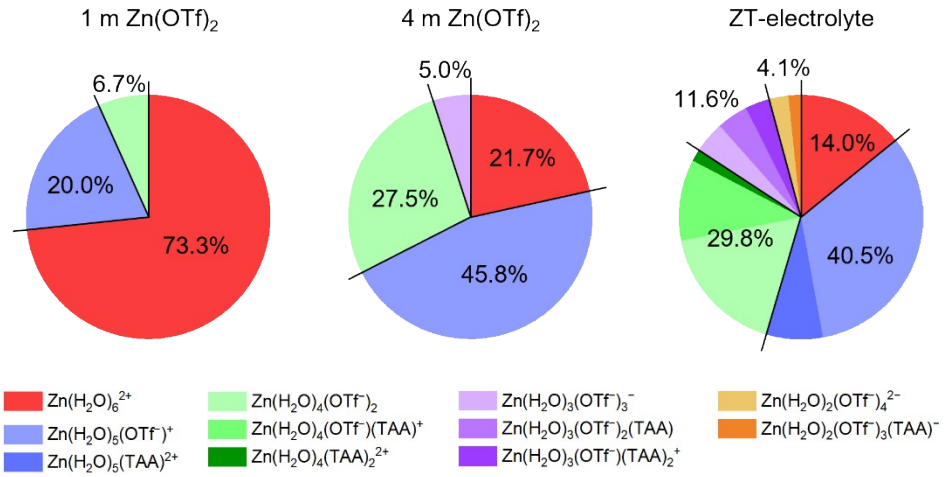

Fig. S10. Coordination complex distribution in the Zn^{2+} solvation structure of the different aqueous electrolytes at 233K.

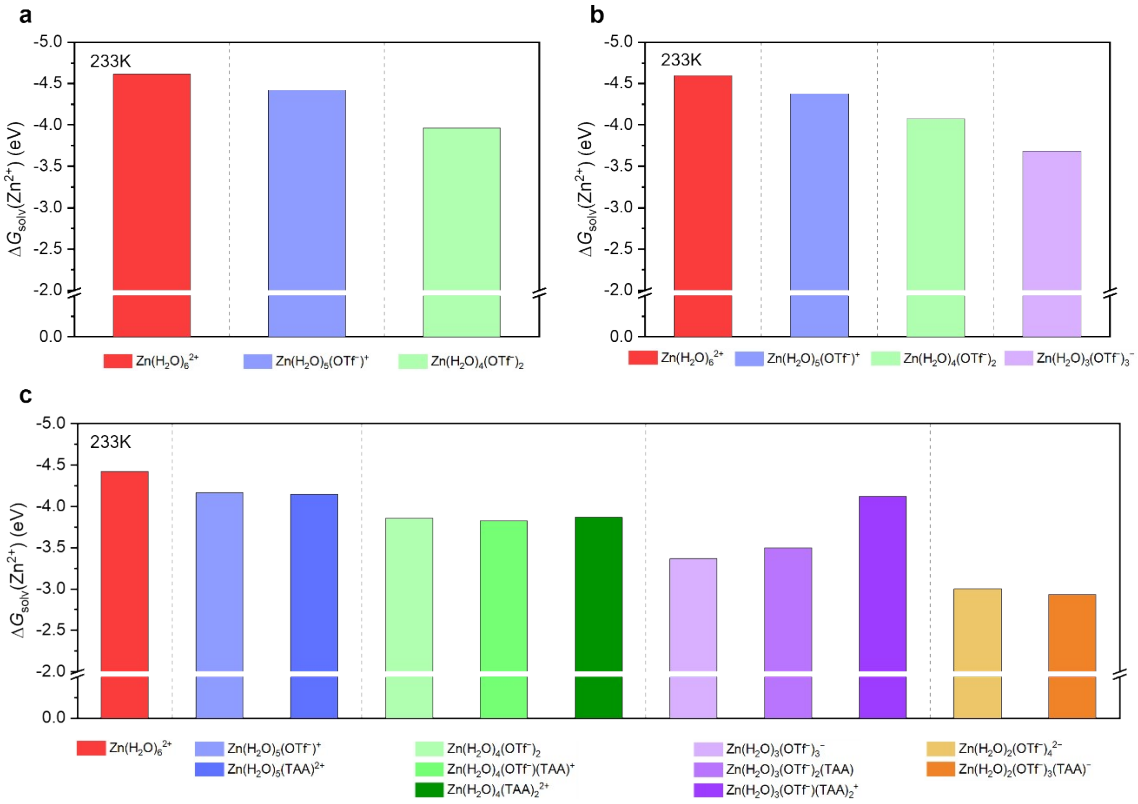

Fig. S11. Solvation free energy (ΔG_{solv}) of the Zn^{2+} in the solvation sheath as a function of coordination complex: 1 m $Zn(OTf)_2$ electrolyte (**a**), 4 m $Zn(OTf)_2$ electrolyte (**b**) and ZT-electrolyte (**c**) at 233K.

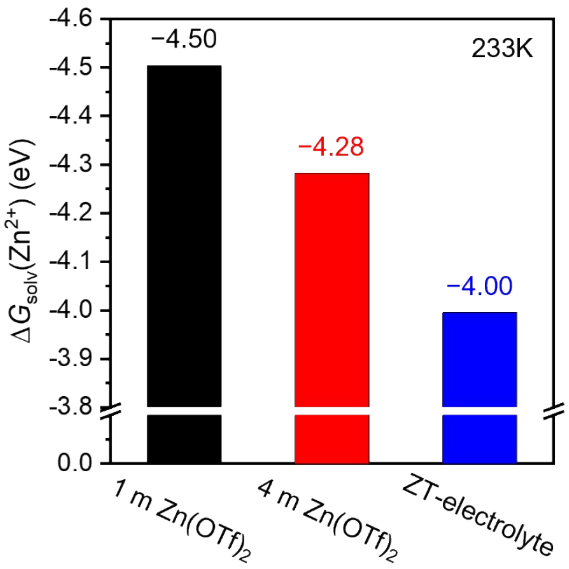

Fig. S12. Comparison of the weighted average value of ΔG_{solv} between the different aqueous electrolytes at 233K

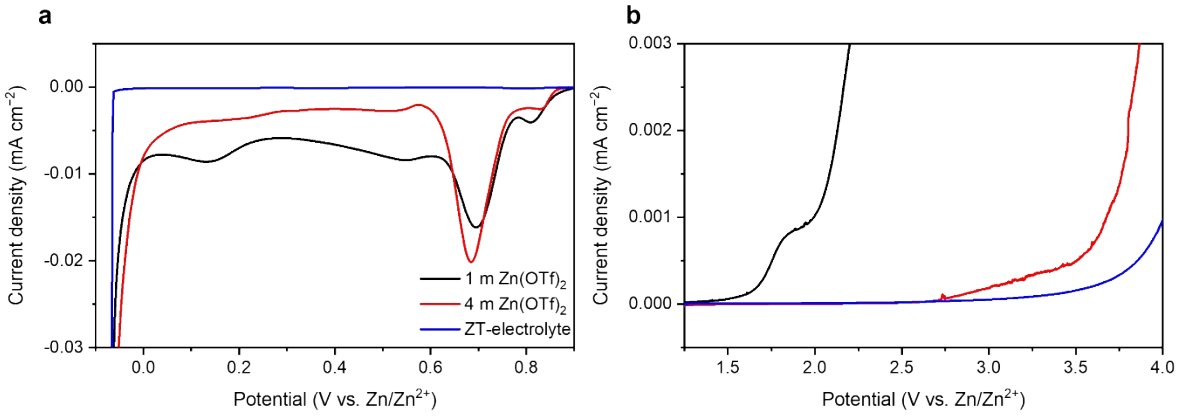

Fig. S13. Electrochemical stability window of the different aqueous electrolytes obtained from the LSV analysis at 1 mV s^{-1} on nonactive Ti electrodes: cathodic stability (**a**) and anodic stability (**b**).

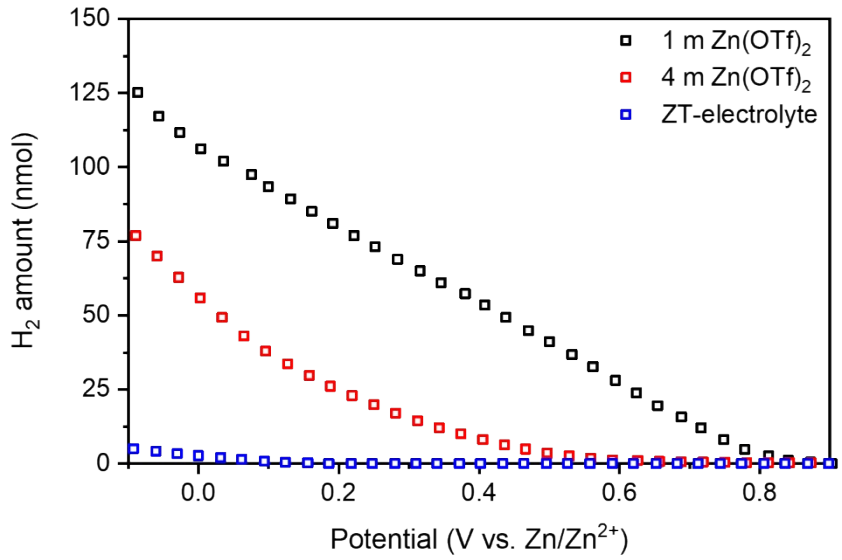

Fig. S14. Hydrogen gas evolution profiles of the different aqueous electrolytes during the LSV analysis, which was obtained using on-line DEMS measurement.

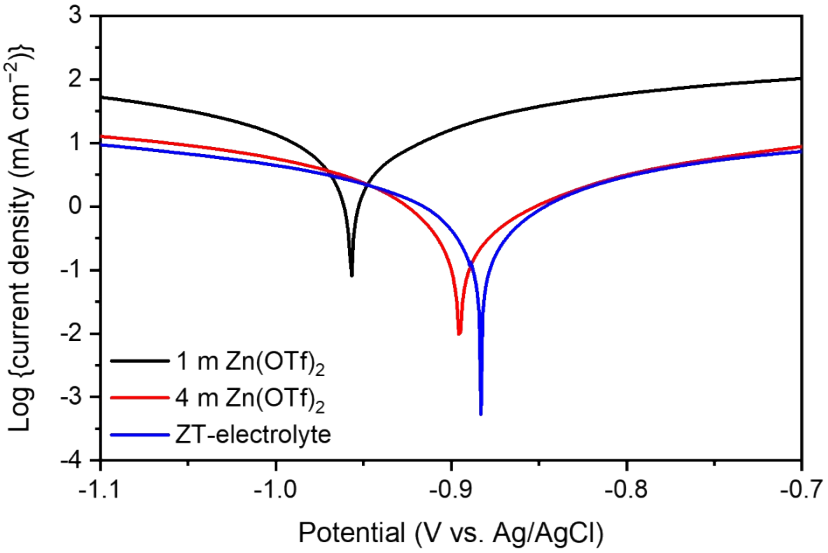

Fig. S15. Tafel plots of the different aqueous electrolytes.

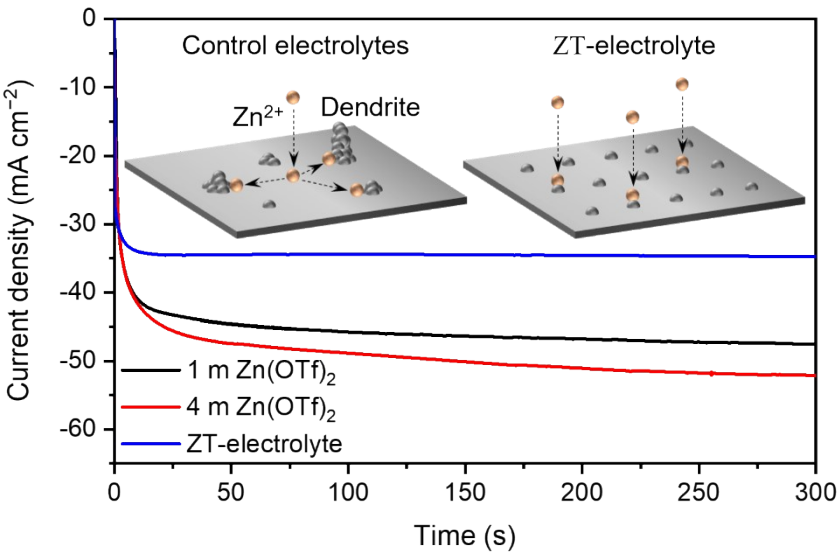

Fig. S16. Chronoamperometry profiles of the different aqueous electrolytes.

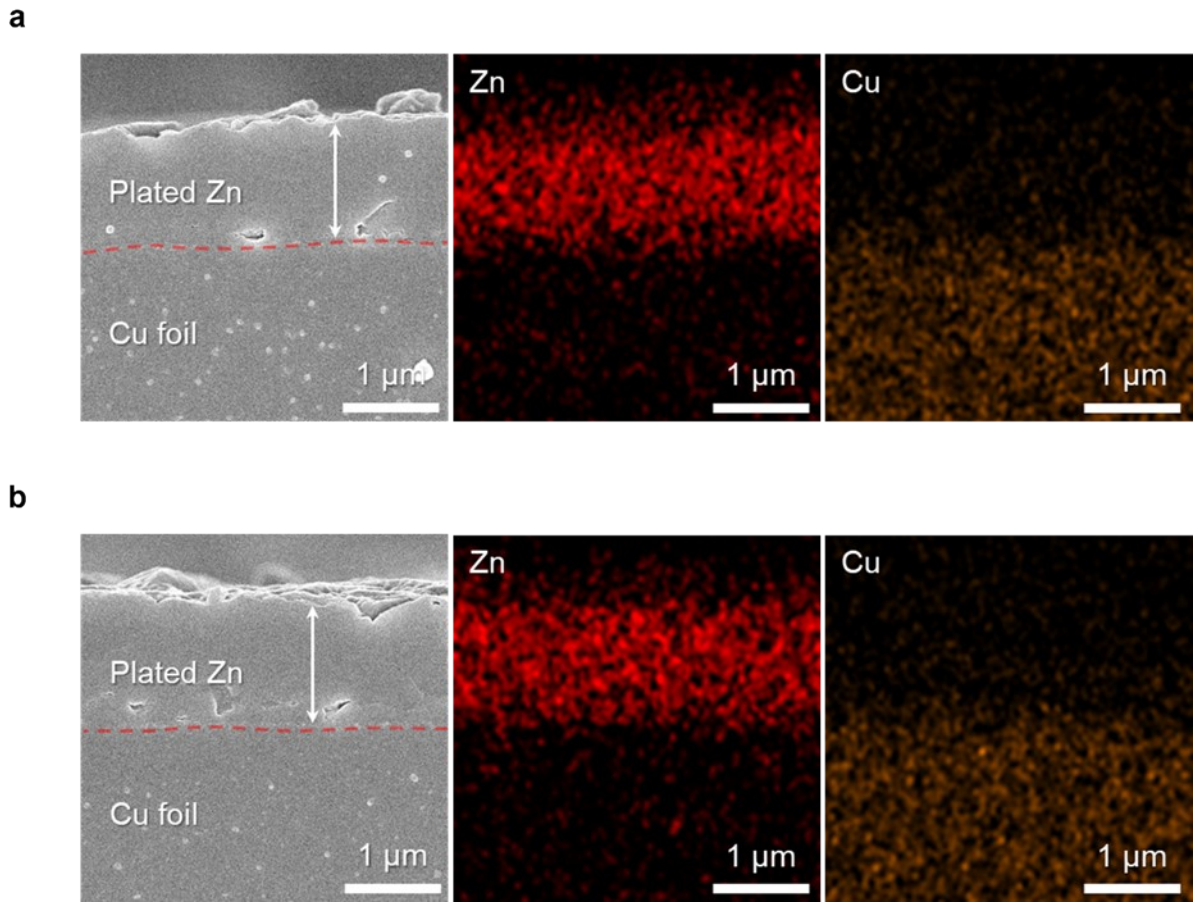

Fig. S17. Cross-sectional SEM images and energy dispersive X-ray spectroscopy (EDS) elemental mapping images of the Zn plated on the Cu foils in the ZT-electrolyte at 25°C (**a**) and −40°C (**b**). The red lines indicate the Zn/Cu interfaces.

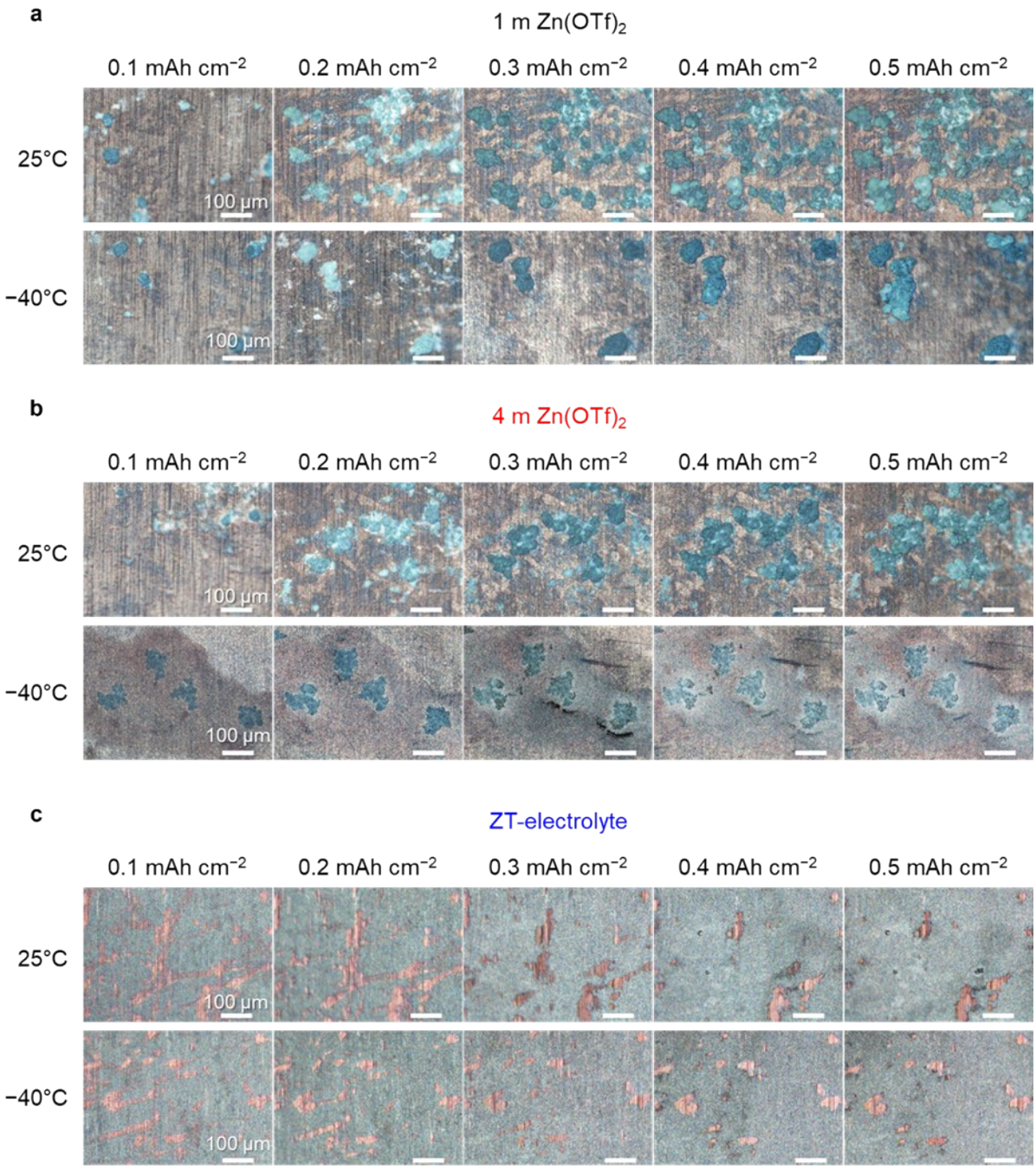

Fig. S18. *In situ* optical microscopy images of the Zn plating process in 1 m $Zn(OTf)_2$ electrolyte (**a**), 4 m $Zn(OTf)_2$ electrolyte (**b**) and ZT-electrolyte (**c**) at 25°C (top) and −40°C (bottom) with 0.2 mA cm^{-2}.

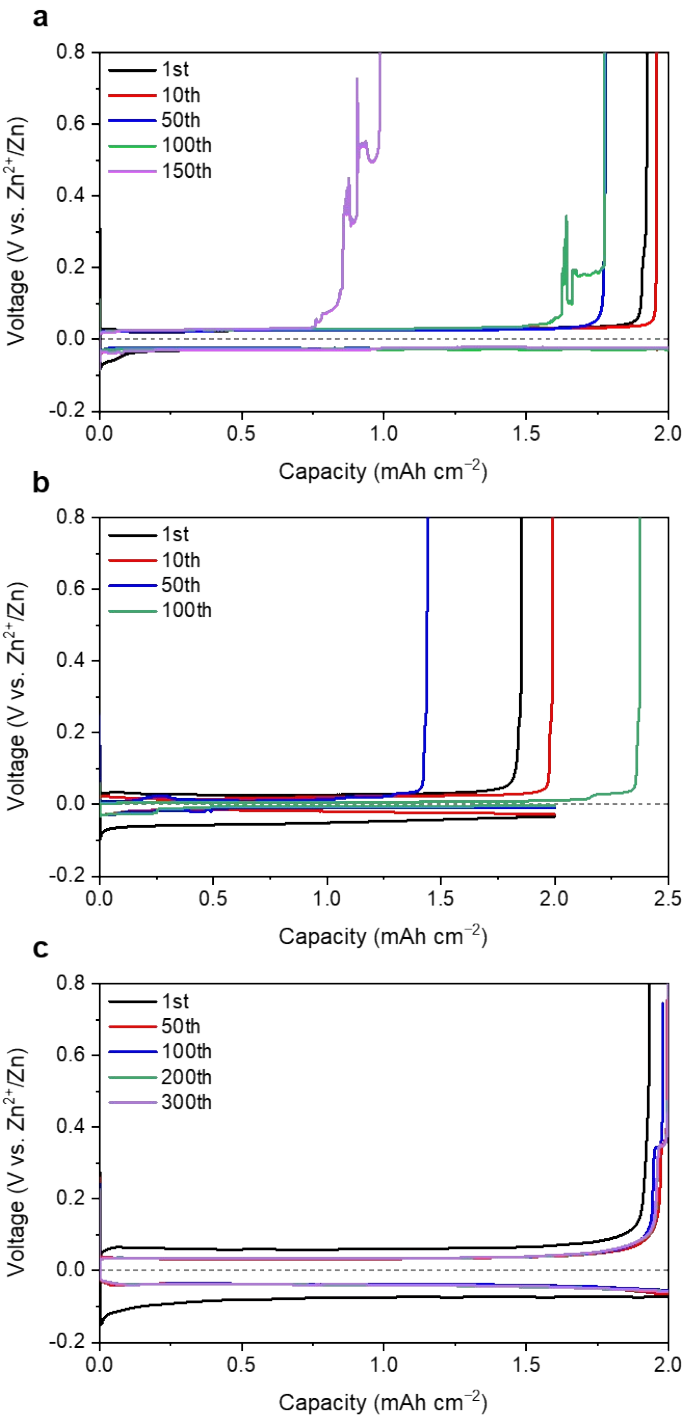

Fig. S19. Galvanostatic Zn plating/stripping profiles of the Zn||Cu asymmetric cells cycled in the 1 m $Zn(OTf)_2$ electrolyte (**a**), 4 m $Zn(OTf)_2$ electrolyte (**b**), and ZT-electrolyte (**c**) at 25 °C with 2.0 mA cm^{-2} and 2.0 mAh cm^{-2}.

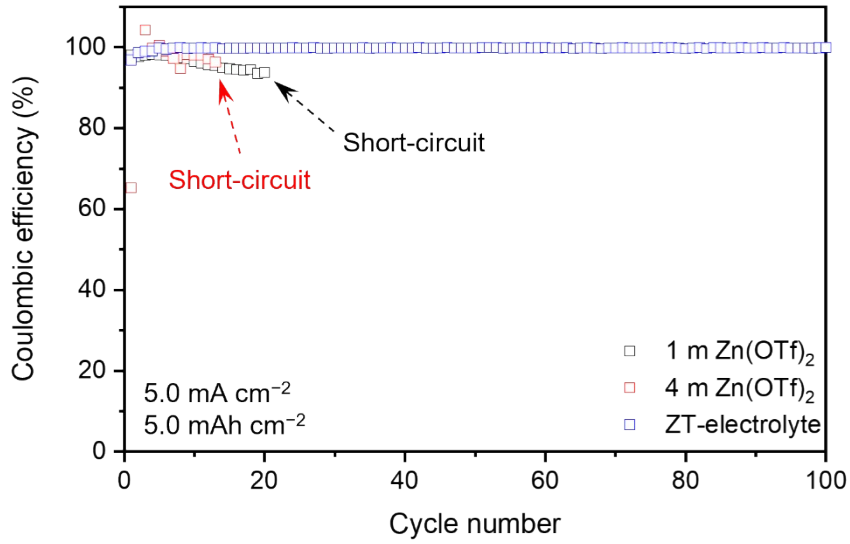

Fig. S20. CE of Zn plating/stripping cyclability in the Zn||Cu asymmetric cells with the different aqueous electrolytes at 25 °C with 5.0 mA cm^{-2} and 5.0 mAh cm^{-2}.

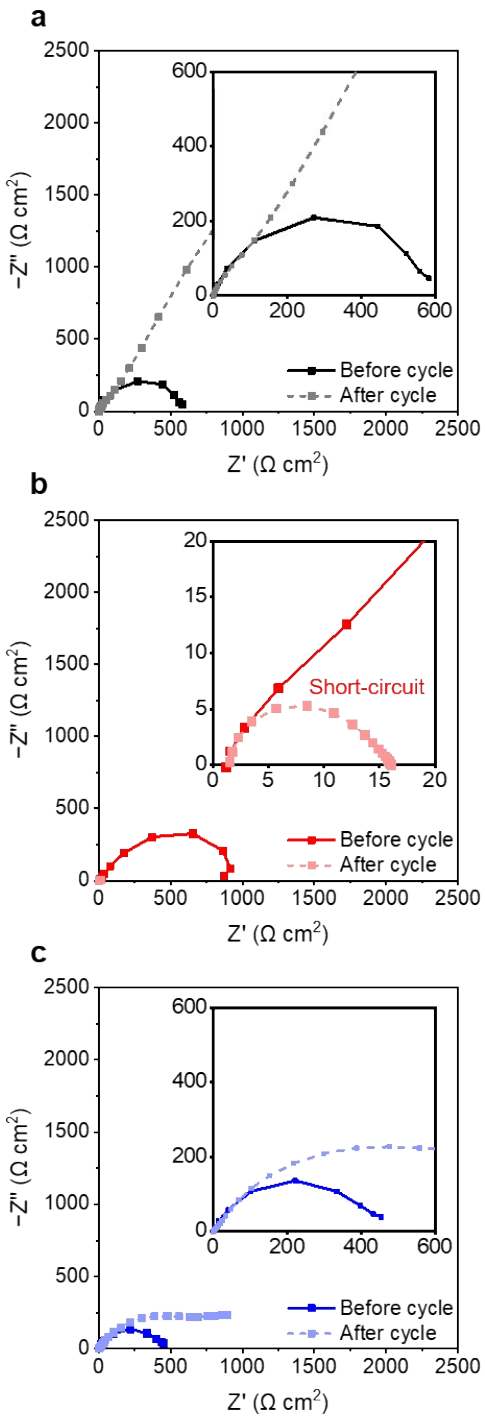

Fig. S21. EIS spectra of the Zn||Zn symmetric cells before and after the plating/stripping cycling test (50 cycles) with 2.0 mA cm^{-2} and 2.0 mAh cm^{-2}: 1 m $Zn(OTf)_2$ electrolyte (**a**), 4 m $Zn(OTf)_2$ electrolyte (**b**), and ZT-electrolyte (**c**) at 25 °C.

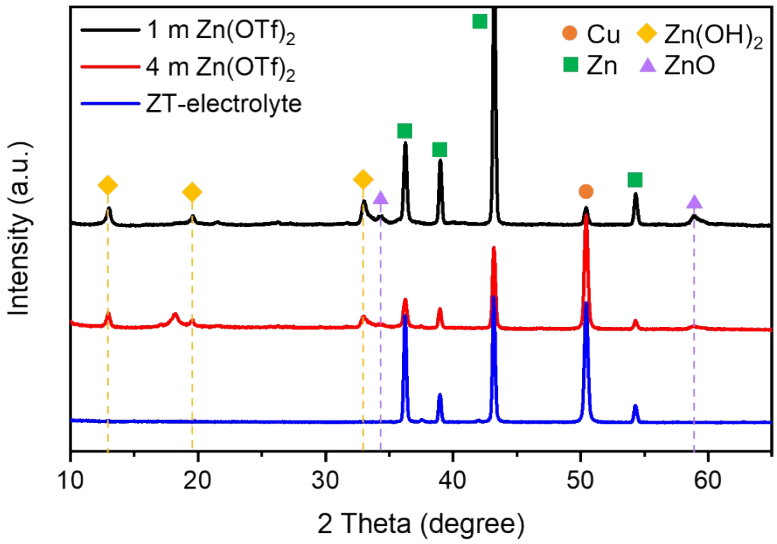

Fig. S22. XRD patterns of the cycled Cu foils (after 50 cycles) in the Zn||Cu asymmetric with the different aqueous electrolytes at 25 °C with 2.0 mA cm^{-2} and 2.0 mAh cm^{-2}.

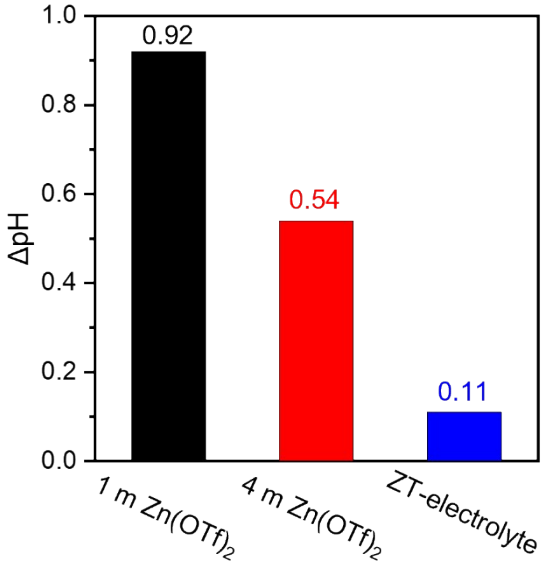

Fig. S23. *In situ* pH analysis of the different aqueous electrolytes during the Zn stripping/plating cycle.

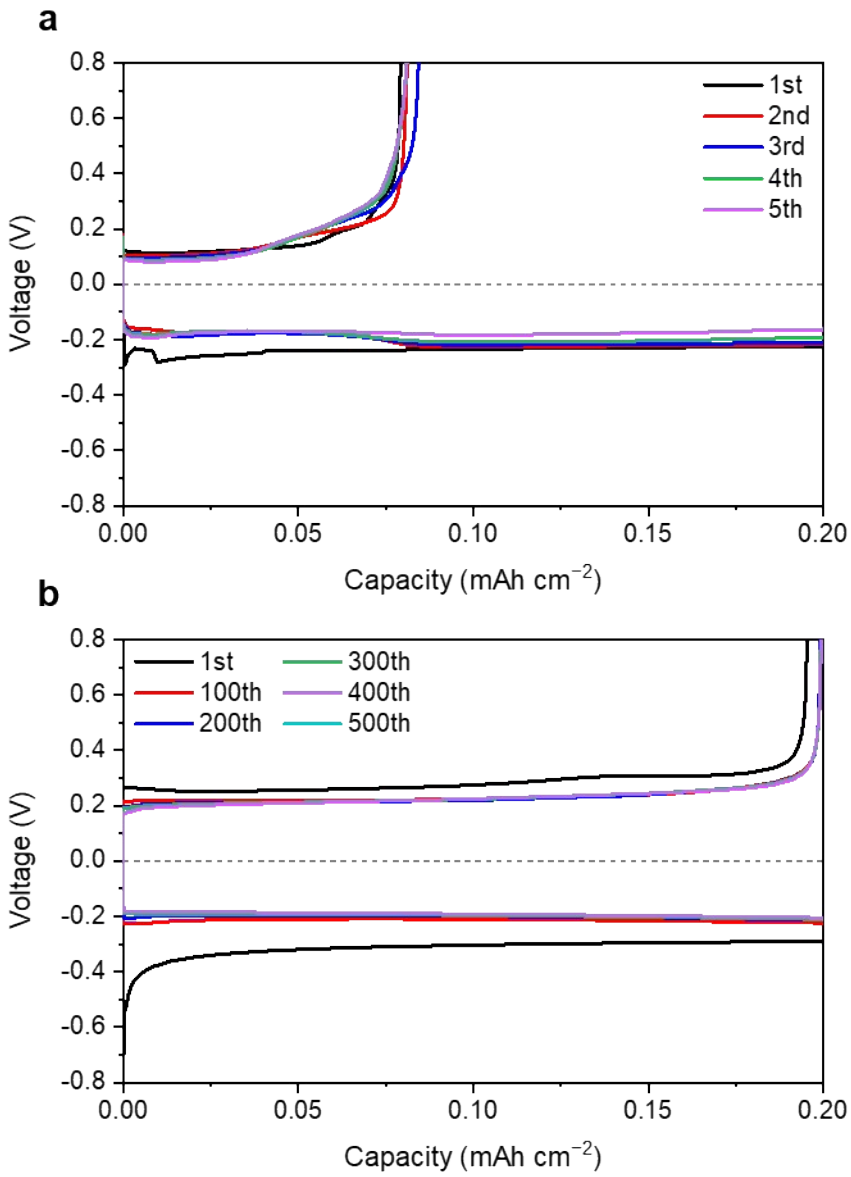

Fig. S24. Galvanostatic Zn plating/stripping profiles of the Zn||Cu asymmetric cells cycled in the 1 m $Zn(OTf)_2$ electrolyte (**a**) and ZT-electrolyte (**b**) at −40°C with 0.2 mA cm^{-2} and 0.2 mAh cm^{-2}.

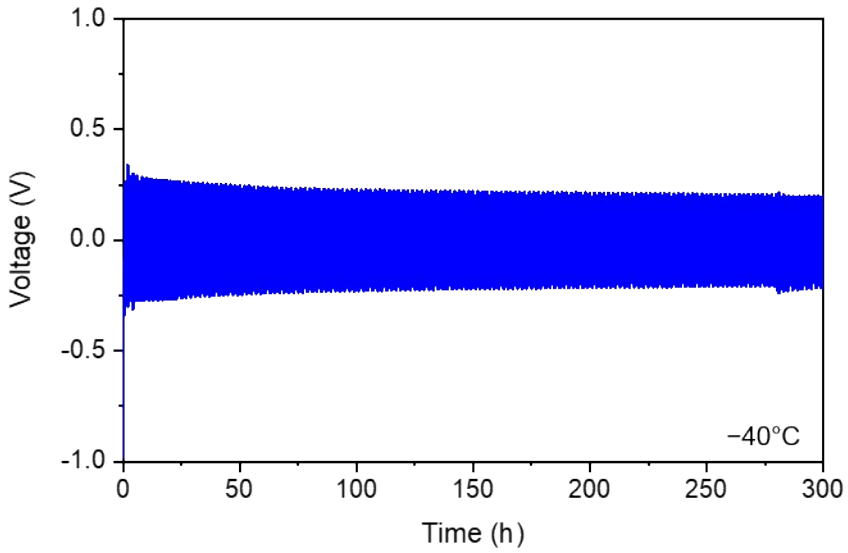

Fig. S25. Galvanostatic Zn plating/stripping profile of the Zn||Zn symmetric cell cycled in the ZT-electrolyte at −40°C with 0.2 mA cm^{-2} and 0.2 mAh cm^{-2}.

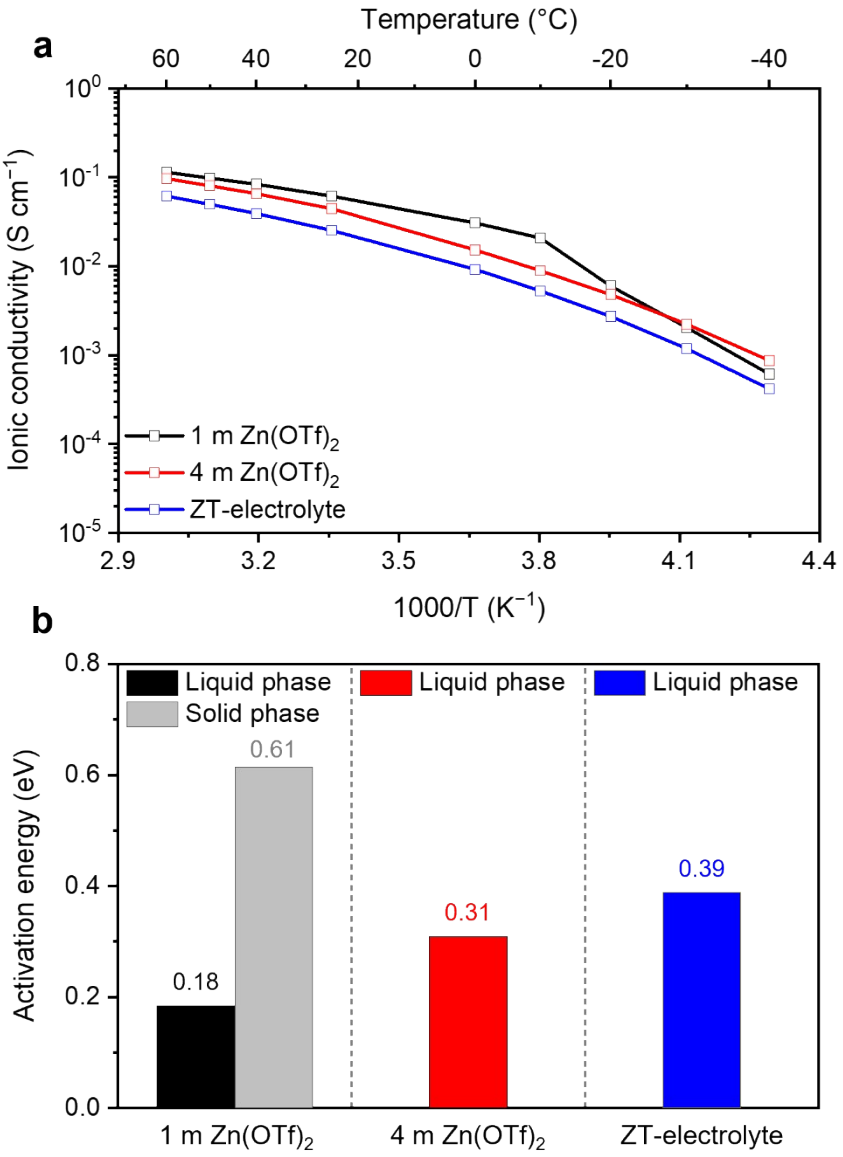

Fig. S26. Ionic conductivity of the different aqueous electrolytes as a function of temperature (**a**) and activation energies in the liquid and solid phases (**b**).

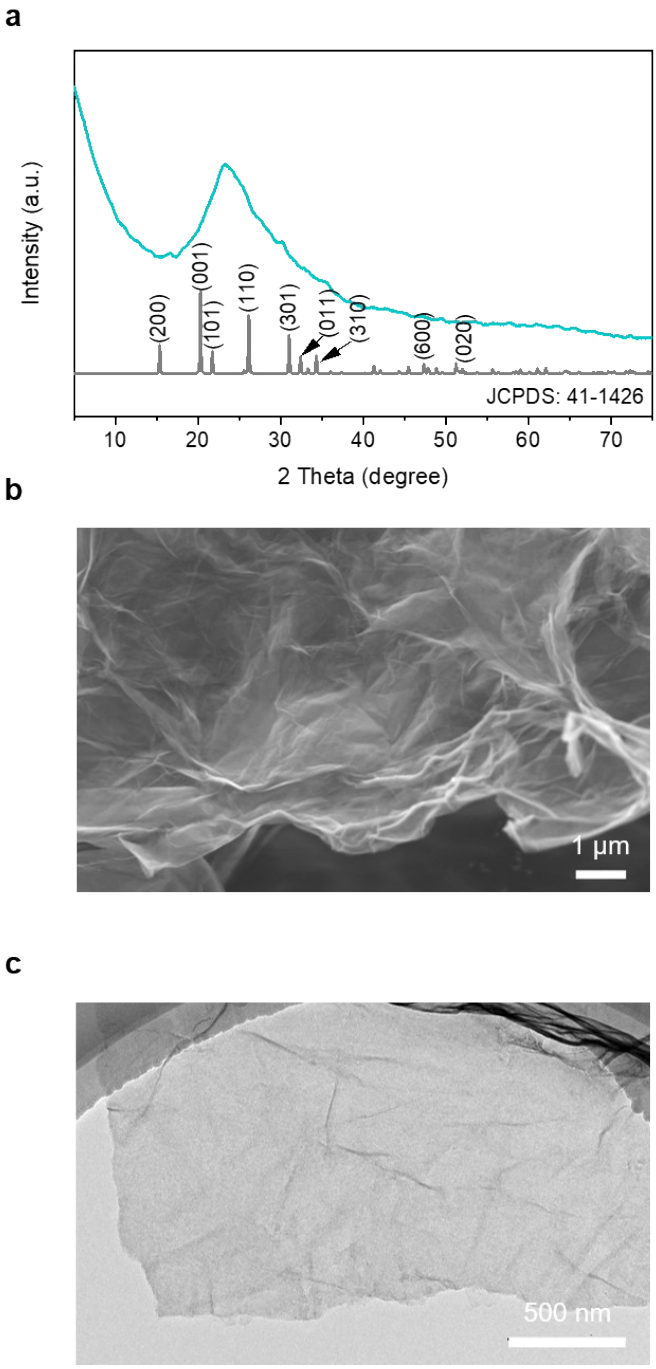

Fig. S27. Characterization of a-V_2O_5@Gr. XRD pattern (**a**), SEM image (**b**) and TEM image (**c**) of a-V_2O_5@Gr.

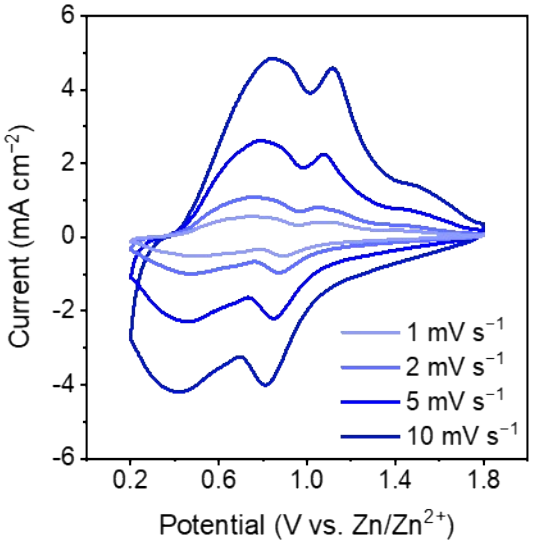

Fig. S28. CV profiles of the Zn||a-V_2O_5@Gr cell with the ZT-electrolyte as a function of scan rate.

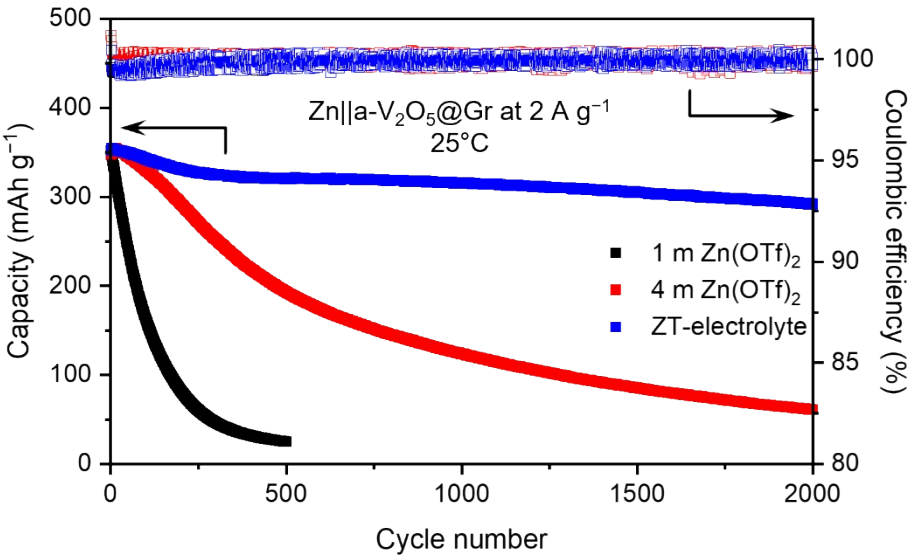

Fig. S29. Cycling performance of the Zn||a-V_2O_5@Gr cells with the different aqueous electrolytes at 25°C with 2 A g^{-1}.

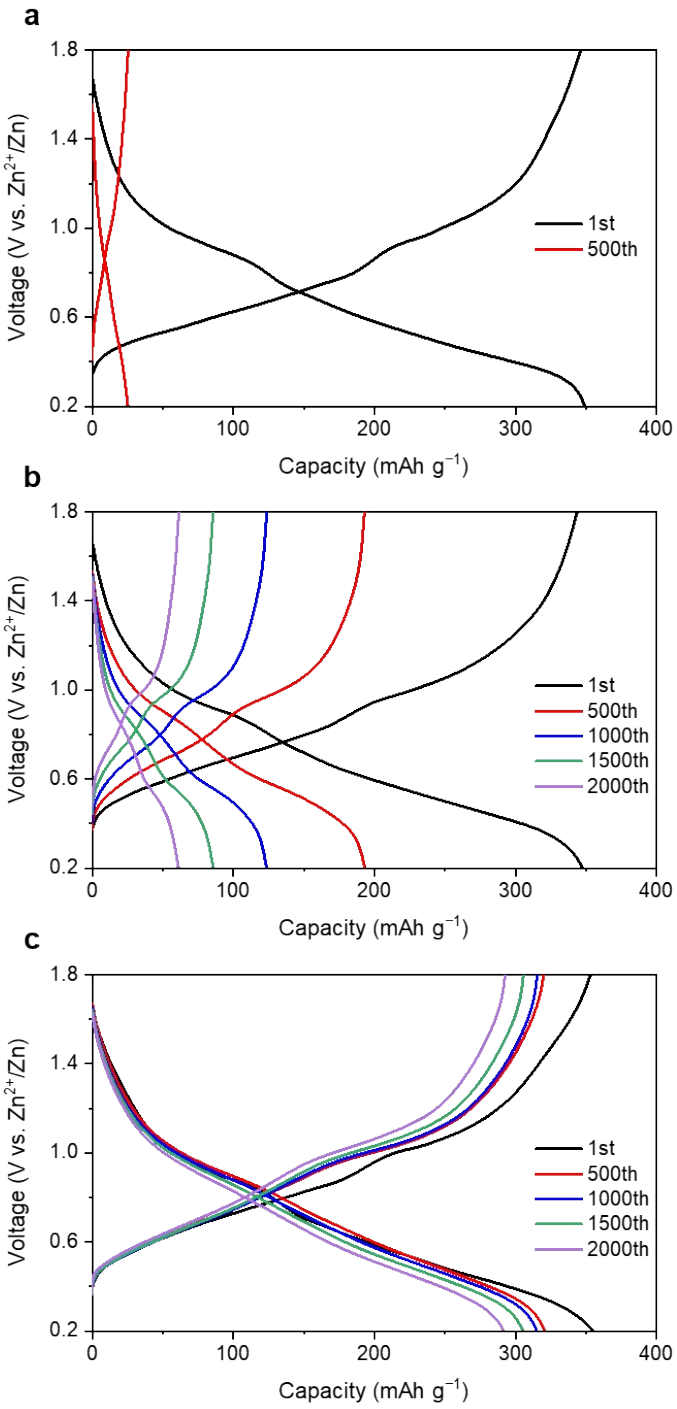

Fig. S30. Charge-discharge voltage profiles of the Zn||a-V_2O_5@Gr cells with the 1 m $Zn(OTf)_2$ electrolyte (**a**), 4 m $Zn(OTf)_2$ electrolyte (**b**), and ZT-electrolyte (**c**) at 25°C with 2 A g^{-1}.

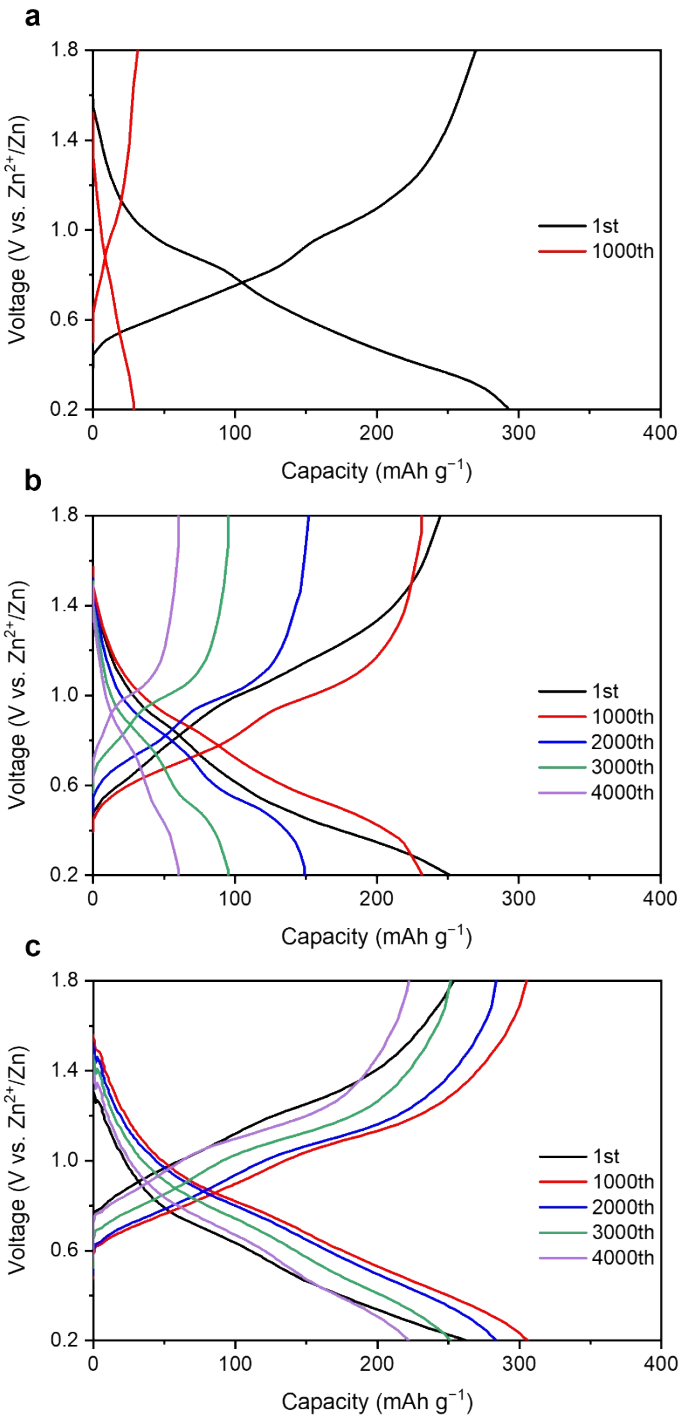

Fig. S31. Charge-discharge voltage profiles of the Zn||a-V_2O_5@Gr cells with the 1 m $Zn(OTf)_2$ electrolyte (**a**), 4 m $Zn(OTf)_2$ electrolyte (**b**), and ZT-electrolyte (**c**) at 25°C with 10 A g^{-1}.

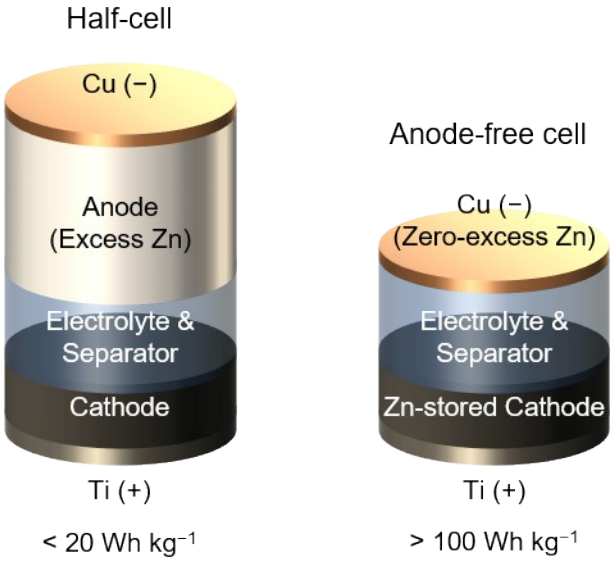

Fig. S32. Schematic illustration of the Zn metal full cell with a large excess of Zn (left) and anode-free cell (right).

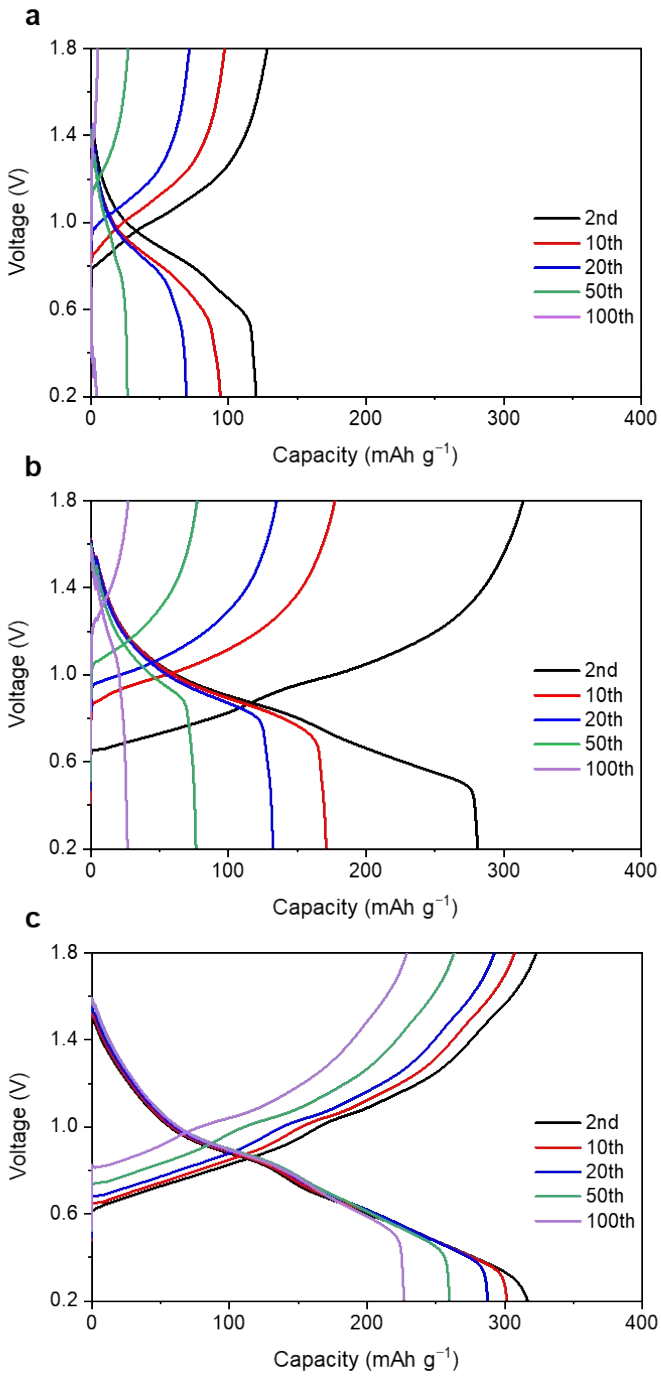

Fig. S33. Charge-discharge voltage profiles of the anode-free Cu||Zn_xa-V_2O_5@Gr cells with the 1 m $Zn(OTf)_2$ electrolyte (**a**), 4 m $Zn(OTf)_2$ electrolyte (**b**), and ZT-electrolyte (**c**) at 25°C with 10 A g^{-1}.

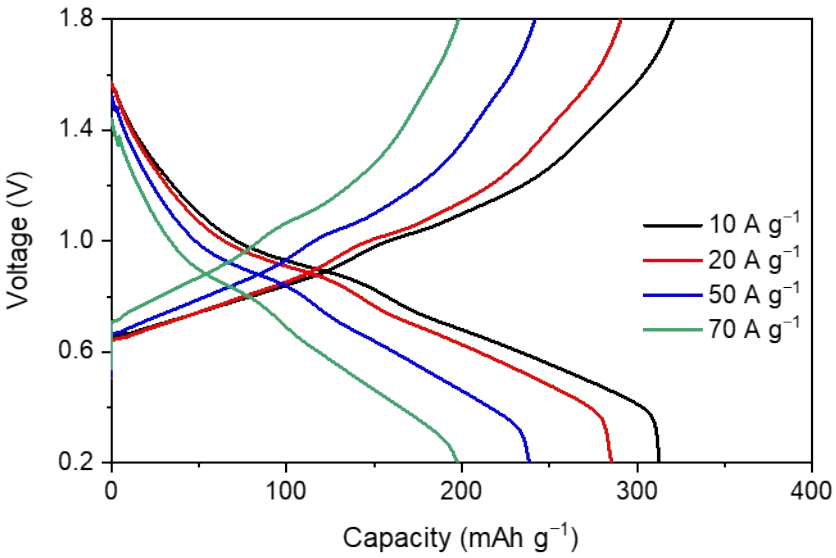

Fig. S34. Charge-discharge voltage profiles of the anode-free Cu||Zn_xa-V_2O_5@Gr cells with the ZT-electrolyte at 25°C as a function of current density.

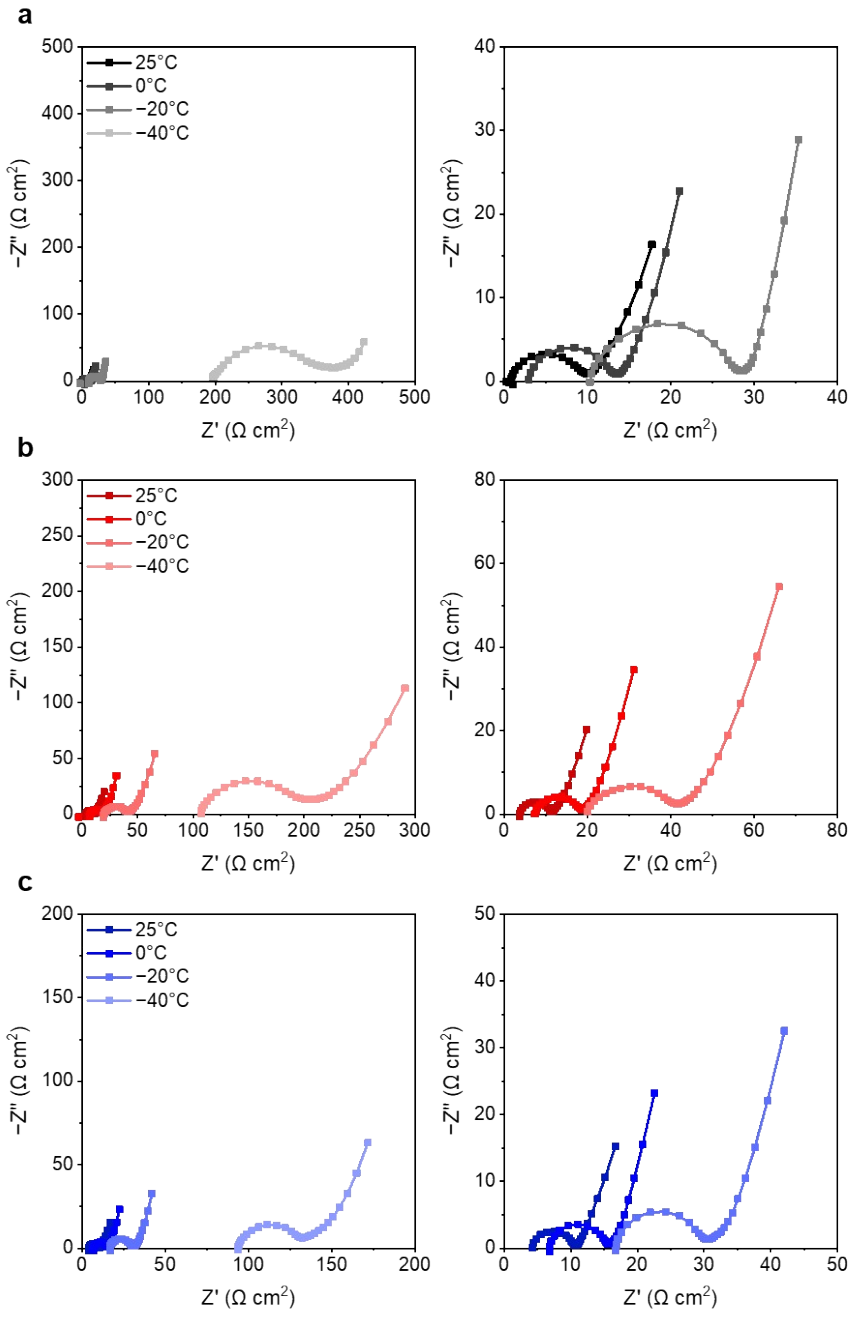

Fig. S35. EIS spectra of the Zn_xa-V_2O_5@Gr||Zn_xa-V_2O_5@Gr (50% DoD) symmetric cells as a function of temperature: 1 m $Zn(OTf)_2$ electrolyte (**a**), 4 m $Zn(OTf)_2$ electrolyte (**b**), and ZT-electrolyte (**c**) at 25 °C.

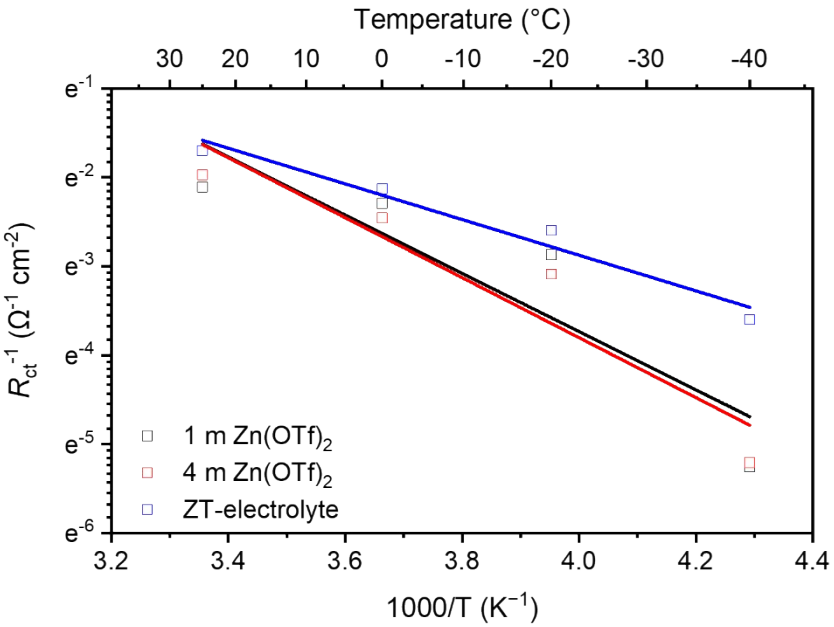

Fig. S36. Arrhenius plot of the R_{ct} for the Zn_xa-V_2O_5@Gr||Zn_xa-V_2O_5@Gr (50% DoD) symmetric cells in the different aqueous electrolytes.

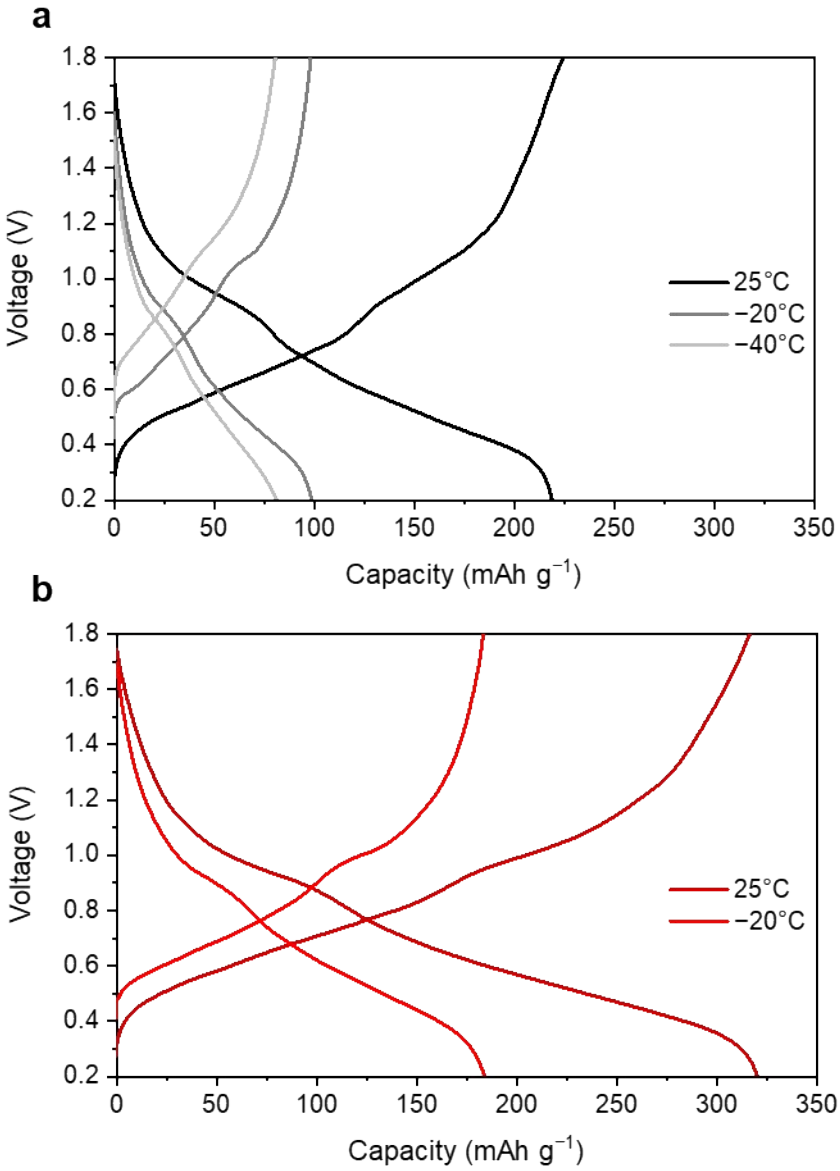

Fig. S37. Charge-discharge voltage profiles of the anode-free Cu||Zn_xa-V_2O_5@Gr cells with the 1 m $Zn(OTf)_2$ electrolyte (**a**) and 4 m $Zn(OTf)_2$ electrolyte (**b**) at different temperatures varying from 25 to −40°C with 200 mA g^{-1}.

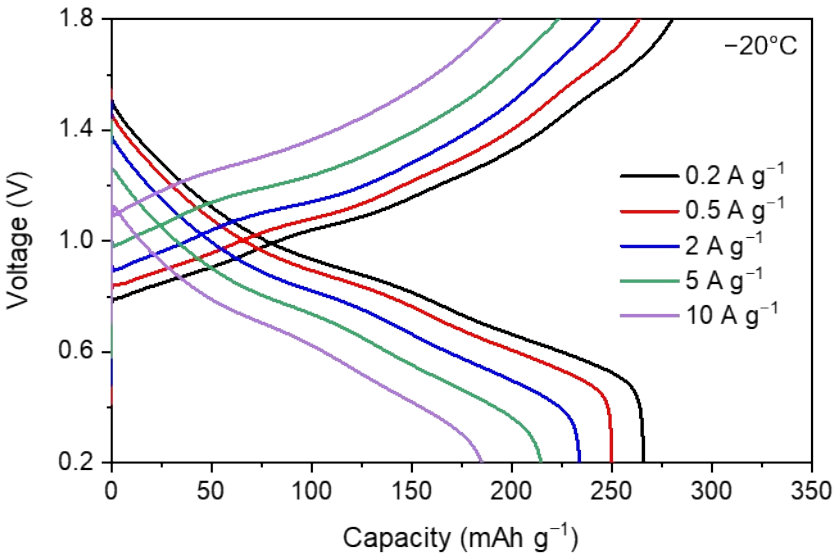

Fig. S38. Charge-discharge voltage profiles of the anode-free Cu||Zn_xa-V_2O_5@Gr cells with the ZT-electrolyte at −20°C as a function of current density.

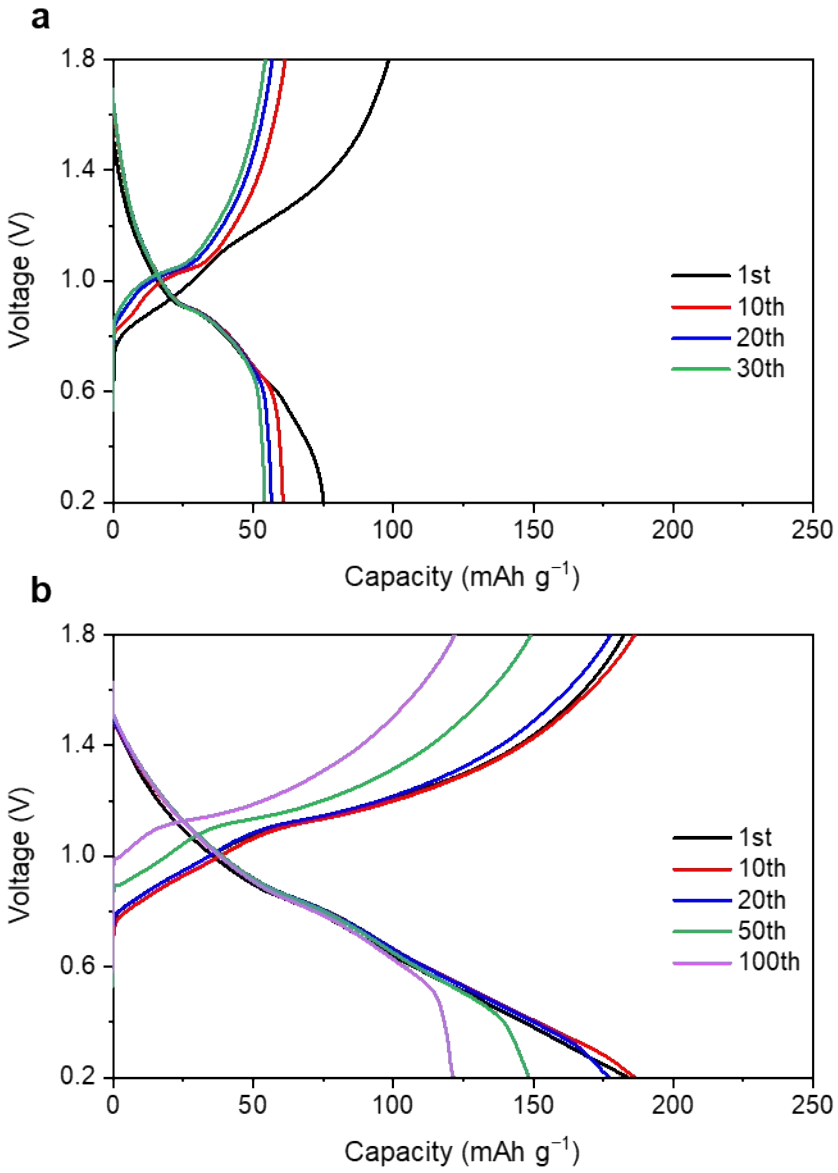

Fig. S39. Charge-discharge voltage profiles of the anode-free Cu||Zn_xa-V_2O_5@Gr cells with the 1 m $Zn(OTf)_2$ electrolyte (**a**) and ZT-electrolyte (**b**) as a function of cycle number at −40°C with 200 mA g^{-1}.

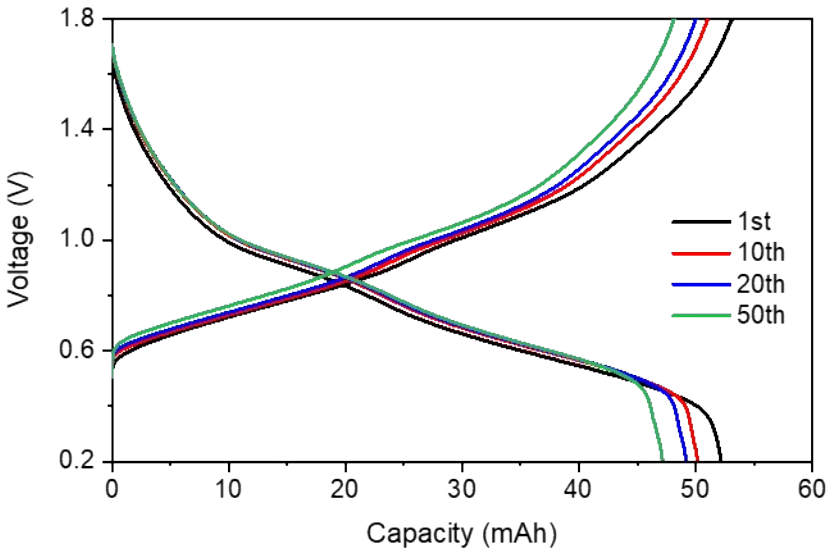

Fig. S40. Charge-discharge voltage profiles of the anode-free Cu||Zn_xa-V_2O_5@Gr pouch cell (115 × 95 mm^2 in size) with the ZT-electrolyte at 25°C with 250 mA g^{-1}.

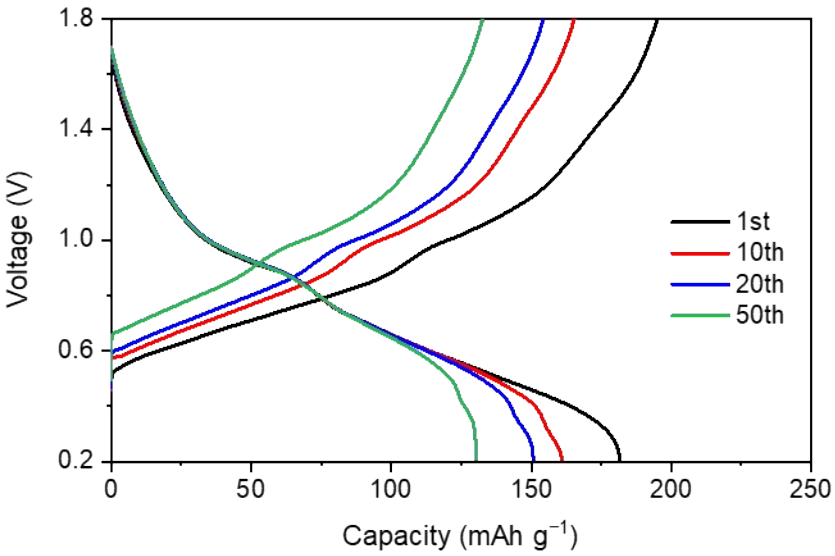

Fig. S41. Charge-discharge voltage profiles of the anode-free Cu||Zn_xa-V_2O_5@Gr pouch cell (30 × 30 mm^2 in size) with the ZT-electrolyte at −40°C with 200 mA g^{-1}.

Tables

Table S1. Comparison in the energy and power densities between this study and the previously reported Zn metal batteries and Li metal batteries. The energy and power densities were calculated based on the total mass of the electrode active materials.

System	Cathode electrode	Anode electrode	Electrolyte	Mass loading of cathode (mg cm^{-2})	Mass loading of anode (mg cm^{-2})	Operating temperature	Operating voltage (V)	Capacity (mAh g^{-1})	Current density (A g^{-1})	Energy density (Wh kg_{total}^{-1})	Power density (W kg_{total}^{-1})	Ref.
Aqueous Zn metal batteries	**Zn_xa-V_2O_5@Gr**	**Cu foil**	**4 m $Zn(OTf)_2$ + 3 m TAA in water**	**1.0−2.0**	**Anode-free**	**RT (25°C)**	**0.98**	**330**	**5**	**231**	**3500**	**This study**
							0.98	**313**	**10**	**219**	**6635**	
							0.98	**285**	**20**	**199**	**12050**	
							0.9	**239**	**50**	**153**	**23242**	
							0.8	**198**	**70**	**113**	**23954**	
						−20°C	**0.98**	**266**	**0.2**	**185**	**112**	
							0.95	**250**	**0.5**	**170**	**257**	
							0.9	**234**	**2**	**150**	**911**	
							0.8	**215**	**5**	**123**	**1858**	
							0.65	**185**	**10**	**86**	**2607**	
						−40°C	**0.9**	**221**	**0.05**	**142**	**22**	

							0.85	**188**	**0.2**	**114**	**69**	
							0.75	**152**	**0.5**	**81**	**123**	
							0.65	**82**	**2**	**38**	**230**	
	$Zn_2(OH)VO_4$	Zn foil	2 M $ZnSO_4$ based gel	4.1	1.5	RT	0.9	200	0.1	115	57	S1
	Polyaniline	Zn foil	7.5 m $ZnCl_2$ in water	17.3	14.3	RT	0.91	150	0.13	64	56	S2
						−20°C	0.91	118	013	50	44	
						−70°C	0.91	65	0.03	28	6	
	$NH_4V_4O_{10}$	Glue-coated Zn	3 M $Zn(OTf)_2$ in water	2.5	7.1	RT	0.7	410	0.1	144	35	S3
	Zn_xVOPO_4	Ti foil	4 m $Zn(OTf)_2$ + 0.5 m $Me_3EtNOTF$ in water	3.0	Anode-free	RT	1.05	135	0.17	118	146	S4
Non-aqueous Zn metal batteries	PQ-MCT	Zn foil	0.5 M $Zn(OTf)_2$ in N, N-dimethylformamide	1.5	21.4	RT	0.75	130	0.2	6	10	S5
						−40°C	0.75	90	0.2	4	7	
						−70°C	0.5	30	0.2	1	2	
	PANI-V_2O_5	Zn foil	2 M $ZnSO_4$ in water:ethylene glycol = 60:40 (v/v)	2.5	35.7	RT	0.9	180	0.1	11	6	S6
						−20°C	0.9	130	0.1	8	4	
	V_2O_5	Zn foil	4 m $Zn(BF_4)_2$ in ethylene glycol	2.5	12.1	RT	0.7	170	0.5	20	60	S7
						−15°C	0.7	100	0.5	12	35	
	$NaV_3O_8·1.5H_2O$	Zn foil	3 M $Zn(OTf)_2$ in	2.0	71.3	RT	0.6	390	0.2	6	3	S8

			water:propylene carbonate = 80:20 (v/v)			−40°C	0.6	183	0.1	3	1	
	E-Bi_2Se_3	Zn foil	0.5 m $Zn(TFSI)_2$ + 10 m LiTFSI in water:ethylene glycol = 50:50 (v/v) with polyacrylamide gel	1.6	107.0	RT	1	231	1	3	15	S9
						−20°C	0.9	301	1	4	17	
Li metal batteries	$LiCoO_2$	Li foil	LiFSI:1,2-dimethoxyethane:1,1,2,2-tetrafluoroethyl 2,2,3,3-tetrafluoropropyl ether = 1:1:3 (mol/mol)	13.5	24.0	RT	4.1	185	0.14	273	206	S10
						−30°C	3.5	150	0.028	189	29	
	SPAN	Li foil	1 M LiFSI in diethyl ether	7.0	1.8	RT	1.6	500	0.17	625	208	S11
						−40°C	1.25	400	0.1	385	77	
						−60°C	1.13	350	0.1	303	61	
	$LiNi_{0.8}Co_{0.1}Mn_{0.1}O_2$	Li foil	1 M $LiPF_6$ in di-fluoro ethylene carbonate:diethyl carbonate = 1:1 (v/v)	6.1	2.7	RT	3.9	180	0.09	501	251	S12
						−30°C	3.9	90	0.09	251	125	
	$LiNi_{0.8}Co_{0.1}Mn_{0.1}O_2$	Li foil	1 M LiFSI in dimethoxyethane:bis(2,2,2 trifluoro ethyl)ether = 1:5 (v/v)	10.5	1.1	RT	3.9	197	0.04	698	140	S13
						−40°C	3.7	129	0.04	434	87	

Table S2. Detailed information of the electrolyte systems for the MD simulation.

Components	Number of H_2O molecules	Number of Zn^{2+} ions	Number of OTf^- ions	Number of TAA molecules	Initial cell parameter (nm^3)
1 m $Zn(OTf)_2$ in H_2O	1665	30	60	−	3.82 × 3.82 × 3.82
2 m $Zn(OTf)_2$ in H_2O	1665	60	120	−	3.95 × 3.95 × 3.95
3 m $Zn(OTf)_2$ in H_2O	1665	90	180	−	4.06 × 4.06 × 4.06
4 m $Zn(OTf)_2$ in H_2O	1665	120	240	−	4.17 × 4.17 × 4.17
4 m $Zn(OTf)_2$ + 1 m TAA in H_2O	1665	120	240	30	4.27 × 4.27 × 4.27
4 m $Zn(OTf)_2$ + 3 m TAA in H_2O	1665	120	240	90	4.46 × 4.46 × 4.46
4 m $Zn(OTf)_2$ + 5 m TAA in H_2O	1665	120	240	150	4.62 × 4.62 × 4.62
4 m $Zn(OTf)_2$ + 7 m TAA in H_2O	1665	120	240	210	4.77 × 4.77 × 4.77

Supplementary references

1 D. Chao, C. Zhu, M. Song, P. Liang, X. Zhang, N.H. Tiep, H. Zhao, J. Wang, R. Wang, H. Zhang, H.J. Fan, *Adv. Mater.*, 2018, **30**, 1803181.

2 Q. Zhang, Y. Ma, Y. Lu, L. Li, F. Wan, K. Zhang and J. Chen, *Nat. Commun.*, 2022, **11**, 4463.

3 Y. Jiao, F. Li, X. Jin, Q. Lei, L. Li, L. Wang, T. Ye, E. He, J. Wang, H. Chen, J. Lu, R. Gao, Q. Li, C. Jiang, J. Li, G. He, M. Liao, H. Zhang, I.P. Parkin, H. Peng, Y. Zhang, *Adv. Funct. Mater.*, 2021, 2107652.

4 L. Cao, D. Li, T. Pollard, T. Deng, B. Zhang, C. Yang, L. Chen, J. Vatamanu, E. Hu, M.J. Hourwitz, L. Ma, M. Ding, Q. Li, S. Hou, K. Gaskell, J.T. Fourkas, X.-Q. Yang, K. Xu, O. Borodin and C. Wang, *Nat. Nanotech.*, 2021, **16**, 902–910.

5 N. Wang, X. Dong, B. Wang, Z. Guo, Z. Wang, R. Wang, X. Qiu and Y. Wang, *Angew. Chem. Int. Ed.*, 2020, **59**,14577–14583.

6 N. Chang, T. Li, R. Li, S. Wang, Y. Yin, H. Zhang and X. Li, *Energy Environ. Sci.*, 2020, 13, 3527.

7 D. Han, C. Cui, K. Zhang, Z. Wang, J. Gao, Y. Guo, Z. Zhang, S. Wu, L. Yin, Z. Weng, F. Kang, Q.-H. Yang, *Nat. Sustain.*, 2022, **5**, 205–213.

8 D.-S. Liu, Y. Zhang, S. Liu, L. Wei, S. You, D. Chen, M. Ye, Y. Yang, X. Rui, Y. Qin, C.C. Li, *Adv. Funct. Mater.*, 2022, **32**, 2111714.

9 Y. Zhao, Y. Lu, H. Li, Y. Zhu, Y. Meng, N. Li, D. Wang, F. Jiang, F. Mo, C. Long, Y. Guo, X. Li, Z. Huang, Q. Li, J.C. Ho, J. Fan, M. Sui, F. Chen, W. Zhu, W. Liu and C. Zhi, *Nat. Commun.*, 2022, **13**, 752.

10 X. Ren, X. Zhang, Z. Shadike, L. Zou, H. Jia, X. Cao, M.H. Engelhard, B.E. Matthews, C. Wang, B.W. Arey, X.-Q. Yang, J. Liu, J.-G. Zhang, W. Xu, *Adv. Mater.*, 2020, 2004898.

11 J. Holoubek, H. Liu, Z. Wu, Y. Yin, X. Xing, G. Cai, S. Yu, H. Zhou, T.A. Pascal, Z. Chen, P. Liu, *Nat. Energy*, 2021, **6**, 303–313.

12 Z. Wang, Z. Sun, Y. Shi, F. Qi, X. Gao, H. Yang, H.-M. Cheng and F. Li, *Adv. Energy Mater.*, 2021, 2100935.

13 J. Holoubek, K. Kim, Y. Yin, Z. Wu, H. Liu, M. Li, A. Chen, H. Gao, G. Cai, T.A. Pascal, P. Liu, Z. Chen, *Energy Environ. Sci.*, 2022, **15**, 1647.